2013

Are 34S-enriched Authigenic Sulfide Minerals a Proxy for Elevated Methane Flux and Gas Hydrates in the Geologic Record?

Walter S. Borowski
Eastern Kentucky University, w.borowski@eku.edu

Nancy M. Rodriguez
Shell

Charles K. Paull
MBARI

William Ussler III
MBARI

Recommended Citation

Borowski, W.S., N.M. Rodriguez, C.K. Paull, William Ussler III. 2013. Are 34S-enriched authigenic sulfide minerals a proxy for elevated methane flux and gas hydrates in the geologic record? Journal of Marine and Petroleum Geology, 43:381-395.

Marine and Petroleum Geology 43 (2013) 381–395

Contents lists available at SciVerse ScienceDirect

Marine and Petroleum Geology

journal homepage: www.elsevier.com/locate/marpetgeo

Are ^{34}S-enriched authigenic sulfide minerals a proxy for elevated methane flux and gas hydrates in the geologic record?

Walter S. Borowski [a,*], Nancy M. Rodriguez [b], Charles K. Paull [c], William Ussler III [c]

[a] Dept. of Geography and Geology, Eastern Kentucky University, Richmond, KY 40475-3102, United States
[b] Shell Production and Exploration, Houston, TX 77079, United States
[c] MBARI, 7700 Sandholdt Road, Moss Landing, CA 95039-0628, United States

ARTICLE INFO

Article history:
Received 27 August 2011
Received in revised form
24 June 2012
Accepted 29 December 2012
Available online 18 January 2013

Keywords:
AOM
Methane
Sulfur isotope
^{34}S enrichment
Sulfide minerals
Gas hydrate

ABSTRACT

The sulfate–methane transition (SMT) zone is a diagenetic transition within anoxic marine sediments created by the metabolic activity of a consortium of sulfate-reducing bacteria and methane-oxidizing *Archaea*. As interstitial dissolved sulfate is consumed by microbially mediated sulfate reduction of sedimentary organic matter (SOM) and anaerobic oxidation of methane (AOM) large enrichments of ^{34}S occur in the interstitial sulfate pool. These isotopic enrichments are transmitted to the dissolved sulfide pool ($\sum HS^-$) and subsequently into sulfide minerals (So, ~FeS, FeS_2).

We investigate the sulfur isotopic composition of pore-water sulfate and sulfide minerals at three sites underlain by gas hydrates at the Blake Ridge. The isotopic composition of sulfate-sulfur is most positive at the SMT showing maximum values of +29.1, 49.6, 51.6‰ VCDT at each of the respective sites. δ^{34}S values of bulk sulfide minerals tend to be more enriched in ^{34}S at and below the SMT ranging from −12.7 to +23.6‰, corresponding to enrichments of 26.7–62.4‰ relative to the mean value of −38.8‰ in the sulfate reduction zone. Both enhanced delivery of methane to the SMT, and non-steady-state sedimentation appear necessary to create large ^{34}S enrichments in sulfide minerals. Similar associations of AOM and large δ^{34}S enrichments (>0‰) occur in other gas hydrate terranes (Cascadia margin) but their exact origin is equivocal at present. An analysis of δ^{34}S data from freshwater and marine sedimentary environments reveals that ^{34}S enrichments within sulfide minerals occur under a range of conditions, but are statistically associated with AOM and systems not limited by dissolved interstitial iron.

In methane-rich sediments, methane delivery to the SMT increases the role of AOM in sulfate depletion that impacts the formation and isotopic composition of authigenic sulfide minerals. We hypothesize that under certain diagenetic conditions large ^{34}S enrichments within sulfide minerals in the geologic record potentially identify: (1) the former occurrence of AOM (2) present-day and "fossil" locations of the sulfate–methane transition zone; and (3) a diagenetic terrane, today characteristic of deep-water, methane-rich, marine sediments conducive to gas hydrate formation. Thus, ^{34}S-enriched sulfide minerals preserved in modern and ancient continental-margin sediments may allow for the identification of AOM-related processes that occur in methane-rich sediments.

1. Introduction

The sulfate–methane transition (SMT) zone is a fundamental boundary between two microbial worlds, separating sulfate-reducers above, and methanogens below. At this transition, sulfate-reducing *Bacteria* and methane-oxidizing *Archaea*, closely related to methanogens (Woese and Fox, 1977), form a consortium (e.g., Hoehler et al., 1994; Orphan et al., 2001), creating a unique diagenetic environment (e.g., Alperin et al., 1988; Borowski et al., 1997; Rodriguez et al., 2000). Here the sulfate reducers and methanotrophs carry out the net process of anaerobic oxidation of methane (AOM):

$$CH_4 + SO_4^{2-} \rightarrow HCO_3^- + HS^- + H_2O.$$

(Reeburgh, 1976, 1983). Sulfate is delivered to the transition zone by diffusing downward through the sediment from overlying seawater while methane, produced deeper within the sediments, diffuses upward. Although the specific biogeochemical pathway of AOM is still not resolved (e.g., Valentine and Reeburgh, 2000;

* Corresponding author. Tel.: +1 859 622 1277; fax: +1 859 622 3375.
E-mail address: w.borowski@eku.edu (W.S. Borowski).

0264-8172/$ – see front matter © 2013 Elsevier Ltd. All rights reserved.
http://dx.doi.org/10.1016/j.marpetgeo.2012.12.009

Hinrichs and Boetius, 2003), the net process produces ^{13}C-depleted dissolved carbon dioxide ($\sum CO_2$ or DIC) derived from methane, and ^{34}S-depleted dissolved sulfide derived from sulfate that ultimately forms authigenic sulfide minerals (e.g., Berner, 1964a, 1970; Jorgensen, 1979; Jorgensen et al., 2004).

We present evidence that accumulations of authigenic sulfide minerals formed within and below the SMT as a result of AOM are enriched in ^{34}S relative to sulfide minerals formed within the overlying sulfate reduction zone in sediments of the Blake Ridge, a region known for possessing methane-rich sediments and gas hydrates. Because the rate of AOM and subsequent precipitation of authigenic sulfide minerals are positively correlated with methane flux (Borowski et al., 1996, 1997, 1999; Niewohner et al., 1998), stratigraphic accumulations of ^{34}S-enriched sulfide minerals should occur at the SMT, and should be preserved in the geologic record as a possible proxy for sustained delivery of methane to the SMT, and the possible co-occurrence of gas hydrates in sediments below.

This simplified view is complicated by a complex interplay of factors including dissolved iron availability and non-steady-state sedimentation that will determine the amount of authigenic sulfide mineral precipitation and their sulfur isotopic composition. A review of the available δ^{34}S data from the literature strengthens the link between AOM and heavy sulfur enrichments in authigenic sulfide minerals, but also shows that these ^{34}S enrichments can occur in several diagenetic environments with differing characteristics. Nonetheless, in a marine sedimentary section the occurrence of ^{34}S-enriched sulfide minerals, in conjunction with other diagenetic indicators of AOM, may be suggestive of present and past methane-rich terranes, which may have also contained gas hydrates.

1.1. Previous work

Continental margin sediments associated with methane gas hydrate deposits – like those of the Blake Ridge region (offshore southeastern North America) – possess distinct diagenetic signals at the base of the sulfate reduction zone (Borowski et al., 1997). In these sediments, consumption of sulfate by AOM within the SMT produces linear sulfate profiles (Fig. 1), reflecting a dynamic relationship between upward methane flux and downward sulfate diffusion toward the transition zone (Borowski et al., 1996). Linear sulfate profiles may not be diagnostic of balanced sulfate and methane co-consumption (see discussion by Kastner et al., 2008, and reply by Dickens and Snyder, 2009), but if steady-state conditions and a 1:1 stoichiometric ratio of methane to sulfate consumption occur (AOM as the predominant sulfate depletion mechanism), the downward sulfate flux calculated from sulfate concentration profiles can be used as a quantitative proxy for methane flux (Borowski et al., 1996; Dickens, 2001). Other than at the Blake Ridge, linear sulfate profiles have been observed on the Amazon Fan (Schultz et al., 1994; Kasten et al., 1998), offshore, western Africa (Schultz et al., 1994; Niewohner et al., 1998), the Gulf of Mexico (Ussler and Paull, 2008), Cascadia (Site U1327D, Wortmann, 2008), the Japan Sea (Snyder et al., 2007a), as well as at numerous DSDP and ODP sites around the world (Borowski et al., 1999). Niewohner et al. (1998); Nambia, Dickens (2001), Blake Ridge and Snyder et al. (2007a,b); Blake Ridge, Japan Sea used diagenetic modeling to confirm a 1:1 stoichiometric relationship between sulfate and methane co-consumption, and the depth to the sulfate–methane transition has since been used as a proxy for gas hydrate distribution (Bhatmagar et al., 2008).

We postulate that the pore-water concentration and isotopic profiles of Blake Ridge sediments (Fig. 1) are representative of other deep-water, methane-rich settings. In these sediments, sulfate, $\sum CO_2$, and alkalinity profiles are linear within most of the sulfate reduction zone. Sulfate concentration decreases, whereas $\sum CO_2$ and alkalinity increase in concentration with depth until reaching the SMT (Borowski et al., 1996, 2000). Near the SMT, alkalinity shows a local increase, reflecting addition of dissolved CO_2 from AOM. Below the SMT, $\sum CO_2$ and alkalinity decrease slightly or remain unchanged before increasing with depth once again several meters below the transition zone. $\delta^{13}C_{\sum CO2}$ values are most negative at the SMT with ^{13}C-depletion as extreme as −37.7‰ PDB (Borowski et al., 2000). Even more extreme ^{13}C-depletion has been measured within an active SMT zone in the Gulf of Mexico ($\delta^{13}C = -63‰$ PDB, Ussler and Paull, 2008).

AOM is a significant sulfate sink, and should impact sulfur geochemistry within and near the SMT. At the Blake Ridge, a large fraction (at least 35%) of total interstitial sulfate is consumed

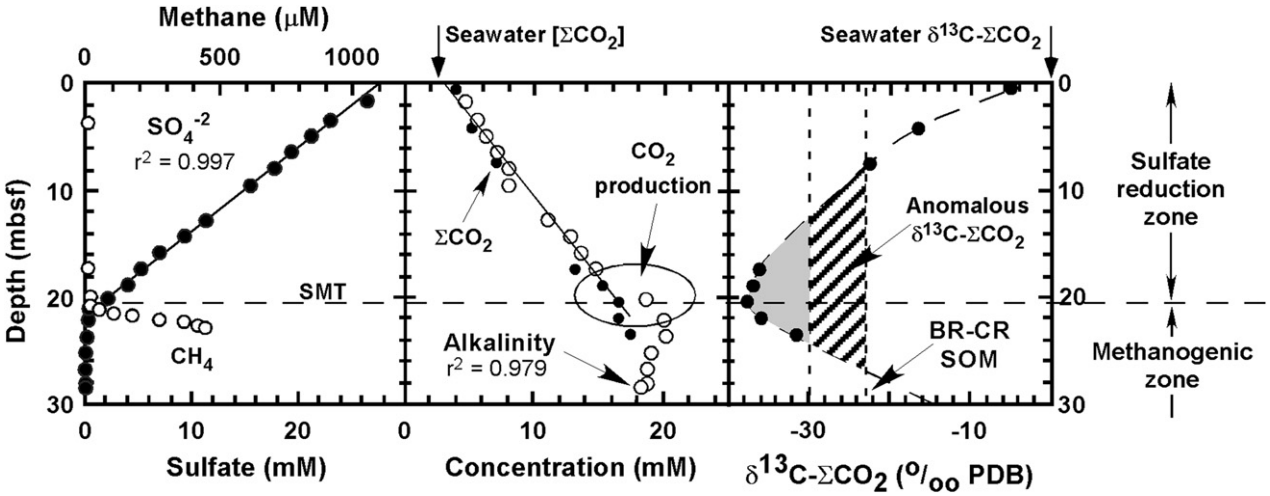

Figure 1. Representative concentration and isotopic profiles of key pore-water constituents from the Blake Ridge (Site 995, ODP Leg 164; Paull et al., 1996). Depth is in meters below seafloor (mbsf). Measurement uncertainties are less than symbol size. In the first panel, note the linearity of the sulfate (filled circles) profile within the sulfate reduction zone and the increase in methane (open circles) concentration below the methanogenic zone. The sulfate–methane transition (SMT) marks the boundary between the sulfate reduction (above) and methanogenic (below) zones. In the middle panel, concentration profiles of dissolved carbon dioxide ($\sum CO_2$) and its proxy, alkalinity (open circles), are shown. The circled portion highlights local production of CO_2 shown by a local increase in alkalinity. In the third panel, the shaded portion of the $^{13}C_{\sum CO2}$ profile identifies the $\sum CO_2$ pool more depleted in ^{13}C than typical marine sedimentary organic matter (SOM) ($\delta^{13}C > -30‰$ PDB; Deines, 1980), and hence carbon derived from methane through anaerobic oxidation of methane. The hachured portion of the $^{13}C_{\sum CO2}$ profile shows carbon likely derived from AOM because the isotopic composition of average SOM in sediments of the Carolina Rise and Blake Ridge is −21‰ (Borowski, 1998; Paull et al., 2000). The lower boundary of the $^{13}C_{\sum CO2}$ profile is defined by a data point (−9.9‰) at 37.65 m below seafloor (mbsf) that is not shown.

through AOM (Borowski et al., 2000) based on numerical modeling of measured methane concentrations above, at, and immediately below the SMT. Niewohner et al. (1998) estimate that 100% of deep sulfate depletion is caused by AOM, and Adler et al. (2000) confirm the steady-state relationship between downward sulfate flux and upward methane flux in Amazon fan sediments.

1.2. Sulfur geochemistry

Sulfur transformations in marine sediments are complex (e.g., Jorgensen, 1983; Fossing and Jorgensen, 1990; Elsgaard and Jorgensen, 1992; Bottrell et al., 2009), but generally sulfate (SO_4^{2-}) derived from seawater is reduced to dissolved hydrogen sulfide ($\sum HS^- = H_2S, HS^-, S^{2-}$), which is ultimately precipitated as sulfide minerals (sulfur, So; iron monosulfides, ~FeS; and pyrite, FeS_2). Decomposition of sedimentary organic matter (SOM) by microbially mediated sulfate reduction depletes the sulfate pool in ^{32}S, generating ^{32}S-enriched dissolved sulfide (e.g., Goldhaber and Kaplan, 1974, 1980). Microbially mediated sulfate reduction has a large isotopic fractionation ($\alpha = 1.029–1.059$; e.g., Chambers and Trudinger, 1978), and the $\delta^{34}S$ values of the sulfate pool typically become distinctly heavier compared to that of the dissolved sulfide pool with continued sediment burial and sulfate reduction (e.g., Kaplan et al., 1963). Dissolved sulfide $\delta^{34}S$ values are typically very light but evolve to heavier values as the sulfate pool is depleted and becomes isotopically heavier (e.g., Goldhaber and Kaplan, 1980). Although the exact pathways of sulfide mineral formation are unresolved (e.g., Berner, 1970; Wilkin and Barnes, 1996; Rickard, 1997; Rickard and Luther, 1997), sulfide minerals are derived from dissolved sulfide produced by sulfate depletion processes (e.g., Berner, 1964a,b, 1970). Final sulfate depletion by AOM localizes production of ^{34}S-enriched $\sum HS^-$ near the SMT that may result in the layered occurrence of authigenic sulfide minerals (e.g., Kasten et al., 1998; Adler et al., 2000). On geologic time scales, elemental sulfur and FeS minerals are ephemeral so that pyrite becomes the predominant solid sulfide phase in sediments and rocks (Berner, 1967; Morse and Cornwell, 1987; Rickard and Luther, 1997). Thus, authigenic sulfide minerals (typically in the form of pyrite) are preserved in the sedimentary record, reflecting the diagenetic environment in which they formed.

2. Methods

Sediments of the Blake Ridge (offshore southeastern North America) were collected by both piston coring (core 11-8, Borowski, 1998), and by coring operations on ODP Leg 164 (sites 994 and 995, Paull et al., 1996). Pore waters were extracted and processed using standard methods (Reeburgh, 1967; Manheim, 1966). Sediment squeeze-cakes created by pore water extraction were sealed in plastic bags and refrigerated. Pore-water sulfate concentration was determined by ion chromatography, and alkalinity was measured onboard by titration (Gieskes et al., 1991). Total dissolved hydrogen sulfide ($\sum HS^- = S^{2-} + HS^- + H_2S$) was measured colorimetrically (Cline, 1969) without allowing anoxic pore waters to oxidize. Total dissolved carbon dioxide ($\sum CO_2$ or DIC) was measured at sea by gas chromatography (Weiss and Craig, 1973), or onshore using cryogenic and manometric techniques (Craig, 1953) from pore-water aliquots stored immediately after squeezing in flame-sealed, airtight ampoules. Methane concentrations from Site 995 pore waters were measured onboard from subcores (Paull et al., 1996), and normalized to pore space volume (Hoehler et al., 2000). Sulfate used for $\delta^{34}S$ measurements was precipitated as $BaSO_4$ using a saturated barium chloride solution. Bulk sedimentary solid-phase sulfide minerals (So, FeS, FeS_2) were extracted from squeeze-cake sediments using the method of Canfield et al. (1986), and precipitated as a single phase (Ag_2S) for gravimetric and isotopic measurements. Reproducibility experiments show that the precision of gravimetric measurements of sulfide mineral concentration is ±0.03%.

Carbon isotopic measurements of $\sum CO_2$ are reported relative to the Pee Dee Belemnite (PDB) standard, and were made using a Delta E mass spectrometer at North Carolina State University (Raleigh, NC). The accuracy and precision of isotopic measurements are ±0.2 and ±0.06‰, respectively (Neal Blair, personal communication).

Sulfur isotopic measurements of interstitial sulfate and bulk sulfide minerals were made at Geochron Laboratories (Cambridge, MA). Barium sulfate samples were thermally decomposed to SO_3, and reduced to SO_2 gas for isotopic measurement (Holt and Engelkemeir, 1970). Measurements were made using a VG Micromass mass spectrometer (Model 903), and are reported relative to the Canyon Diablo Troilite (VCDT) standard. Measurement precision is ±0.1‰ and cumulative precision of the extraction process and isotopic measurement is ±0.3‰ (Marshall Otter, personal communication).

3. Results

Pore-water sulfate concentration decreases linearly with depth at each site (Table 1, Fig. 2). Based on sulfate concentration data, the depth of the sulfate–methane transition (SMT) is 10.3, ~20, and ~21 mbsf at sites 11-8, 994, and 995, respectively. In general (see a discussion of the exceptions below), the $\delta^{34}S$ values of interstitial sulfate become more positive as sulfate concentrations decrease with sediment depth to the SMT (Table 1; Fig. 2). Sulfate is maximally enriched in ^{34}S at or immediately above the sulfate–methane transition with $\delta^{34}S$ ranging from +29.1‰ VCDT (piston core 11-8, Fig. 2) to +51.6‰ (Site 995, Fig. 2). The amount of ^{34}S enrichment within sulfate ranges from 8.1 to 30.6‰, relative to seawater sulfate values (+21‰ CDT, Rees et al., 1978). The exceptions to these general trends are 7 data points near the SMT (appearing in italics in Table 1) where smaller $\delta^{34}S$ values occur below a maximum in the profile. We interpret these values as artifacts resulting from dissolved sulfide being oxidized to sulfate because we did not acidify and shake pore waters to remove dissolved hydrogen sulfide. Thus, ^{34}S-depleted sulfide was oxidized to sulfate and incorporated into a ^{34}S-enriched sulfate pool to generate bulk sulfate values less than peak $\delta^{34}S$-$_{SO4}$ values observed in the sediments above. This isotopic artifact is quantitatively consistent with low interstitial sulfate concentrations observed at the SMT. Alternatively, these values could represent *in situ* oxidation of sulfide to sulfate (e.g., Aller and Rude, 1988; Fossing and Jorgensen, 1990) but no such instances have been reported for deep-water, continental margin sediments for samples in the shallow sedimentary section that have been properly handled after collection (e.g., Bottrell et al., 2000 observed sulfide oxidation within Cascadia sediments only at significantly deeper depths well below the SMT associated with a subsurface source of sulfate).

Although dissolved sulfide concentrations were not measured at the ODP sites, $\sum HS^-$ was measured in samples from 69 piston cores collected from sites in the same region of the Blake Ridge and Carolina Rise (Borowski, 1998). The mean $\sum HS^-$ concentration is 3 ± 14 μM ($N = 494$) ranging between 0 and 113 μM with a median value of <1 μM; only 29 of 494 dissolved sulfide measurements are >6 μM (Fig. 3A). Data from core 11-8 shows these characteristic low $\sum HS^-$ concentrations (Fig. 3B), as do other cores near the ODP drill sites (Borowski, 1998). Because of generally low $\sum HS^-$ concentrations, we have no measurements of the sulfur isotopic composition of the dissolved sulfide pool.

The weight abundance of sulfur residing in bulk sulfide minerals generally increases with depth within the sulfate reduction zone

Table 1
Concentration and isotopic data for pore-water and solid-phase sulfur species measured from piston core 11-8 and ODP Sites 994 and 995 on the Blake Ridge.

Site	Sample	Depth (mbsf)	Sulfate[a] (mM)	δ^{34}S-sulfate (‰ VCDT)	Weight % sulfide sulfur	δ^{34}S-sulfide minerals (‰ VCDT)
11-8[b]	54–60	0.57	26.1	20.2	0.03	−39.3
	54–60[c]	0.57	–	19.9	0.03	–
	54–60[c]	0.57	–	–	0.03	–
	133–139	1.36	27.3	–	0.04	–
	233–239	2.36	23.4	21.8	0.11	−46.4
	233–239[c]	2.36	–	–	0.14	–
	340–346	3.43	19.7	–	0.08	–
	440–446	4.43	17.0	23.9	0.09	−40.2
	540–546	5.43	14.6	–	0.06	–
	648–654	6.51	12.2	24.6	0.03	–
	648–654[c]	6.51	–	–	0.04	−31.2
	648–654[c]	6.51	–	–	0.03	–
	748–754	7.51	8.6	25.5	0.12	–
	848–854	8.51	4.9	27.4	0.13	–
	956–962	9.61	2.1	29.1	0.08	−33.6
	956–962[c]	9.61	–	–	0.09	–
	1056–1062	10.59	0.0	–	0.14	23.6
	1056–1062[c]	10.59	–	–	0.14	–
	1156–1162	11.59	0.0	–	0.14	5.3
	1156–1162[c]	11.59	–	–	0.15	–
	1262–1268	12.65	0.0	–	0.30	3.4
	1262–1268[c]	12.65	–	–	0.37	–
	1362–1368	13.65	0.0	–	0.30	−21.7
	1462–1468	14.65	0.0	–	0.17	−36.7
	1475–1490	14.82	0.6	–	0.12	−35.7
	1475–1490[c]	14.82	–	–	0.14	–
994A[b]	1H1 140–150	1.40	25.6	23.9	0.11	−26.1
	1H2 140–150	2.90	23.9	–	0.11	−46.0
	1H3 140–150	4.40	22.7	27.2	0.23	−46.6
	1H4 140–150	5.90	23.2	–	0.11	–
	1H5 140–150	7.40	20.6	31.4	0.28	−42.1
	2H1 140–150	9.30	14.4	35.7	0.18	−35.4
	2H2 140–150	10.80	12.9	–	0.21	–
	2H3 140–150	12.30	11.1	39.2	0.29	−36.6
	2H3 140–150[c]	12.30	–	–	–	−38.4
	2H4 140–150	13.80	9.2	–	0.55	–
	2H5 140–150	15.30	6.8	45.0	0.34	−35.5
	2H6 140–150	16.80	5.1	49.6	0.54	–
	3H1 140–150	18.80	4.1	*34.2*[d]	0.42	−35.0
	3H2 10–25	19.00	–	–	0.45	–
	3H2 45–60	19.35	–	*37.7*[d]	0.60	–
	3H2 80–95	19.70	–	–	0.42	–
	3H2 115–130	20.05	–	–	1.22	–
	3H2 140–150	20.30	1.2	*31.7*[d]	0.47	−30.7
	3H2 140–150[c]	20.30	–	–	–	−28.7
	3H-3 10–25	20.50	–	–	0.32	−26.9
	3H-3 45–60	20.85	–	*21.9*[d]	0.54	−32.1
	3H-3 80–95	21.20	–	–	0.43	−27.0
	3H-3115–130	21.55	–	–	0.39	−17.9
	3H-3140–150	21.80	1.3	–	0.32	−17.7
	3H-4140–150	23.30	0.7	–	0.40	−12.7
	3H-5140–150	24.80	0.2	–	0.21	−13.9
	3H-5140–150[c]	24.80	–	–	–	−14.5
	3H-6140–150	26.30	0.6	–	0.37	−14.5
	3H-6140–150[c]	26.30	–	–	–	−15.5
	3H-6140–150[c]	26.30	–	–	–	−14.6
	4H-2140–150	28.89	1.0	–	0.68	−3.2
	4H-3140–150	30.39	1.4	–	0.84	–
	4H-4140–150	31.89	0.2	–	0.71	−8.1
	4H-5140–150	33.39	0.8	–	0.52	–
	4H-6140–150	34.89	1.0	–	0.42	18.8
995A[b]	3H1 153–158	12.70	11.2	–	0.37	−44.1
	3H2 150–155	14.25	9.2	–	0.53	−42.4
	3H2 150–155[c]	14.25	–	–	–	−38.0
	4H3 145–150	25.15	0.0	–	0.58	–
	4H4 145–145	26.65	0.0	–	0.50	–
	4H5 145–150	28.15	0.0	–	0.90	–
	5H5 145–150	37.65	0.0	–	1.51	−6.3
995B	1 H-1 38–48	0.38	–	21.2	0.04	−8.4
	1H1 85–95	0.85	–	–	0.19	−19.5
	1H2 0–15	1.50	–	–	0.14	−25.9
	1H2 140–150	2.90	27.0	22.5	–	–
	1H3 108–118	4.08	23.6	26.2	0.15	−46.4
	1H4 140–150	5.90	21.7	–	0.40	–
	1H5 140–150	7.40	19.9	29.7	0.16	−35.5
	2H-1140–150	17.40	6.0	44.5	0.48	−36.5
	2H-2140–150	18.90	3.0	48.1	0.69	−35.3
	2H-3140–150	20.40	1.6	51.6	0.33	−23.5
	2H-4 10–20	20.60	–	–	–	−14.6
	2H-4 15–20	20.65	–	–	0.34	–
	2H-4 15–20[c]	20.65	–	–	0.32	−16.7
	2H-4 30–40	20.80	–	–	–	–
	2H-4 72–82	21.22	–	*26.2*[d]	0.30	−15.2
	2H-4 72–82[c]	21.22	–	–	0.31	−15.7
	2H-4 92–102	21.42	–	–	0.44	−12.2
	2H-4 92–102[c]	21.42	–	–	0.35	−12.4
	2H-4122–132	21.72	–	*19.2*[d]	–	–
	2H-4140–150	21.90	0.0	–	0.26	−11.2
	2H-5140–150	23.40	0.0	–	0.37	−17.9
	2H-5140–150[c]	23.40	–	–	–	−19.0
	2H-5140–150[c]	23.40	–	–	–	−17.1
	2H-6140–150	24.90	0.5	–	0.38	−16.9

[a] Sulfate concentration data for piston core 11-8 from Borowski (1998); for ODP sites from Paull et al. (1996).
[b] Sulfate–methane transition (SMT) zone depths for core 11-8, Site 994, and Site 995 are 10.3, 21, and 21 m, respectively.
[c] Replicate analyses.
[d] δ^{34}S values affected by dissolved sulfide oxidation.

(Fig. 2). The amount of sulfide minerals tends to be higher at and below the SMT than within the sulfate reduction zone. In the case of Site 994, a distinct peak of sulfide-mineral sulfur (1.2 wt%) occurs at the SMT, coincident with increased concentrations of $CaCO_3$ and authigenic dolomite depleted in ^{13}C (Rodriguez et al., 2000). Values of $\delta^{34}S_{\text{sulfide mineral}}$ range from −46.6 to +23.6‰ across the entire sedimentary interval (0–40 mbsf), but values at and immediately below the SMT are enriched in ^{34}S relative to values in the overlying sulfate reduction zone (Fig. 2). Distinct peaks of $\delta^{34}S_{\text{sulfide mineral}}$ occur at sites 11-8 and 995 coincident with the SMT. At Site 994, ^{34}S enrichments within sulfide minerals continue with depth below the SMT, reaching a maximum at 34.89 mbsf. The mean value of $\delta^{34}S_{\text{sulfide mineral}}$ within the sulfate reduction zone is −34.0 ± 10.3‰ (ranging from −46.6 to −8.4‰; median = −35.5‰; $N = 27$). Below the SMT, mean values of $\delta^{34}S_{\text{sulfide mineral}}$ are −14.5 ± 13.5‰ (ranging from −36.7 to +23.6‰; median = −15.3‰; $N = 32$). Maximum $\delta^{34}S_{\text{sulfide mineral}}$ values near the SMT range from −12.7 to +23.6‰, corresponding to ^{34}S enrichments of 26.7 and 62.4‰, relative to the mean value of −38.8‰ in the overlying sulfate reduction zone.

4. Discussion

4.1. $\delta^{34}S$ of sulfate and sulfide minerals

The ultimate source for sulfur within dissolved sulfide and authigenic sulfide minerals is seawater sulfate. Depletion of interstitial sulfate occurs by both oxidation of SOM and by AOM. Microbes mediating these processes preferentially use ^{32}S, creating an isotopically heavier residual sulfate pool (more positive $\delta^{34}S$ values) and an isotopically lighter dissolved sulfide pool (more negative $\delta^{34}S$ values) (e.g., Chambers and Trudinger, 1978). Because taxonomically related sulfate-reducing microbes presumably mediate both sulfate-consuming processes (e.g., Orphan et al., 2001), we assume the magnitude of isotopic fractionation for both sulfate

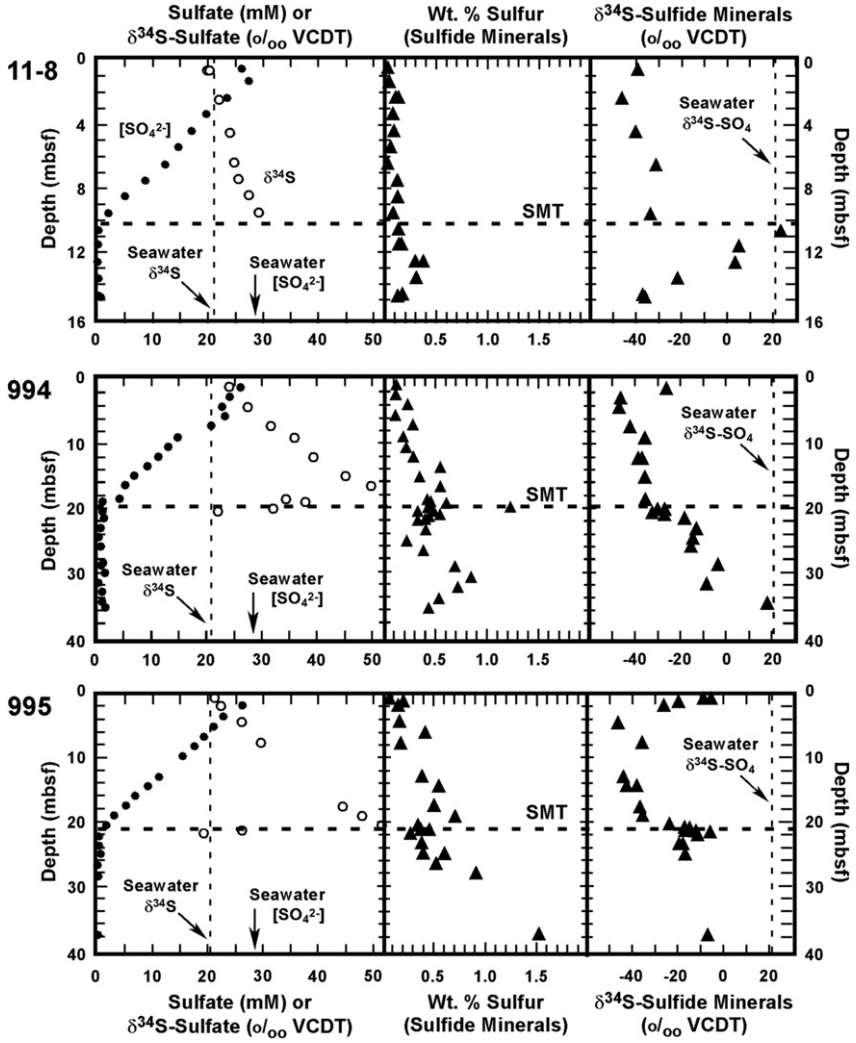

Figure 2. Profiles of interstitial dissolved sulfate (SO_4^{2-}), sulfur isotopic composition of pore-water sulfate ($\delta^{34}S_{SO4}$) in per mil (‰) relative to the Canyon Diablo Troilite (VCDT), sulfur content of sediments residing in bulk sulfide minerals (collectively native sulfur, iron monosulfides, and pyrite) expressed in weight percent sulfur (wt%), and sulfur isotopic composition of sedimentary sulfide minerals ($\delta^{34}S_{sulfide\ minerals}$) at piston core site 11-8 and Ocean Drilling Program sites 994 and 995. The sulfur isotopic composition of modern seawater sulfate is shown by dashed vertical lines. Dashed horizontal lines indicate the sulfate–methane transition (SMT) zone as defined by interstitial sulfate and methane concentrations. Sulfate concentrations from the ODP sites are from Paull et al. (1996). Open triangles in the first panel for ODP Sites 994 and 995 depict $\delta^{34}S_{SO4}$ values affected by sulfide oxidation.

depletion mechanisms are similar. The observed ^{34}S enrichment of interstitial sulfate with depth (Table 1, Fig. 2) is qualitatively consistent with either mechanism of sulfate reduction, however the isotopic composition of bulk sulfide minerals provides clues into the location and mechanism of sulfide mineral formation.

The transfer of sulfur from dissolved sulfide into sulfide minerals occurs with a fractionation of only ~1‰ (Price and Shieh, 1979; Wilkin and Barnes, 1996). Sulfate enriched in ^{34}S should not only lead to relative ^{34}S enrichments in dissolved sulfide, but also to ^{34}S enrichments of approximately equal magnitude in sulfide minerals. Thus, dissolved sulfide and sulfide minerals will be depleted in ^{34}S relative to the interstitial sulfate pool, but enriched in ^{34}S relative to dissolved sulfide and sulfide minerals formed shallower in the sulfate reduction zone. We have no sulfur isotopic measurements of $\sum HS^-$ because of low interstitial concentrations (usually <6 μM; Fig. 3), so we cannot directly compare the sulfur isotopic composition of dissolved sulfide and solid-phase sulfide. These low concentrations suggest that dissolved sulfide quickly enters the solid phase as iron sulfide minerals (as observed by Adler et al., 2000). Thus, we infer that the availability of dissolved iron is not a primary limitation for the formation of iron sulfide minerals within Blake Ridge sediments.

We infer that sulfide mineral formation occurs in distinct stratigraphic zones via different diagenetic processes (Fig. 4). Sulfide minerals in continental-margin sediments are typically depleted in ^{34}S and may display extreme depletions ($\delta^{34}S = -40$ to -50‰ CDT) presumably due to microbial sulfur disproportionation (Canfield and Thamdrup, 1994), additional sulfur cycling in the uppermost sulfate reduction zone (Aller and Rude, 1988; Fossing and Jorgensen, 1990; Elsgaard and Jorgensen, 1992; Habicht and Canfield, 2001), and/or slow sulfate reaction rates (Sim et al., 2011). These large depletions in ^{34}S form a background signal or baseline to which heavy sulfur is added as sulfate reduction progresses with increasing depth in the sulfate reduction zone. Minima in $\delta^{34}S_{sulfide\ mineral}$ values occur at 2.36, 4.40, and 4.08 mbsf at sites 11-8, 994, and 995 respectively, produced by sulfur disproportionation and sulfide oxidative processes. Below these depths, $\delta^{34}S$ values increase toward the SMT as heavy sulfide-sulfur generated by sulfate reduction enters iron sulfide minerals. Our data collectively show that as pore water sulfate becomes enriched

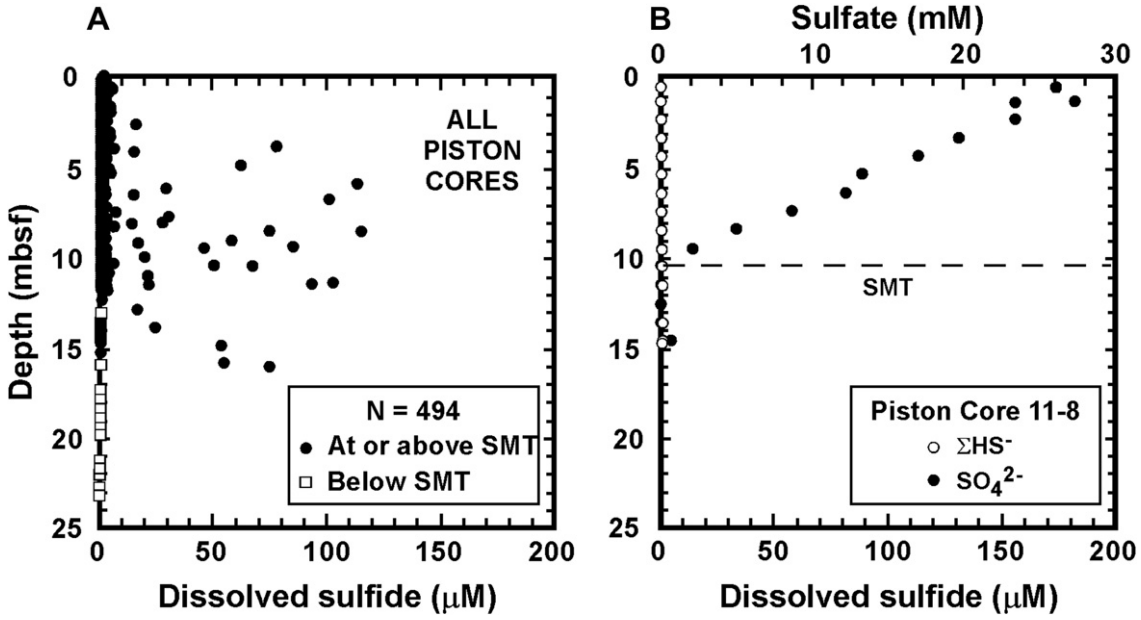

Figure 3. Concentration of dissolved sulfide ($\sum HS^- = H_2S, HS^-, S^{2-}$) of pore waters extracted from piston cores in Blake Ridge region (Borowski, 1998). Depth is in meters below seafloor (mbsf). Note the stratigraphic location of the sulfate–methane transition (SMT) zone. In Graph A, sediment samples taken above the SMT are shown with filled circles whereas samples taken below the SMT are shown with open squares. Mean and median $\sum HS^-$ concentrations are 3 ± 14 μM and <1 μM, respectively in (μM = micromoles per liter). Samples with higher interstitial sulfide concentration (>10 μM) generally occur at sites proximal to salt diapirs and generally are not representative of sediments over the expanse of the Blake Ridge and Carolina Ridge, with a few exceptions (Borowski, 1998). The preponderance of the data (465 of 494 samples) shows interstitial sulfide concentrations of less than 6 μM, suggesting that dissolved sulfide produced by sulfate reduction and AOM quickly enters the solid phase. Graph B shows the concentrations of dissolved sulfide ($\sum HS^-$, open symbols) and sulfate (SO_4^{2-}; filled circles) of piston core 11-8. Note linear sulfate profile with complete sulfate depletion at ~10 mbsf, and very low $\sum HS$ concentrations even at and below the SMT. No dissolved sulfide data exist at ODP Sites 994 and 995, but their interstitial sulfide concentration profiles are presumed similar to that of core 11-8.

in ^{34}S during its depletion, the $\delta^{34}S$ signal of sulfide minerals concomitantly becomes more positive approaching the SMT (Fig. 2).

Larger amounts of sulfide minerals occur near and below the SMT relative to inventories in overlying sediments (Fig. 2). We attribute this increase in sulfide minerals at or near the SMT to the local, sustained production of dissolved $\sum HS^-$ by AOM, and its subsequent precipitation with dissolved interstitial iron. Perhaps

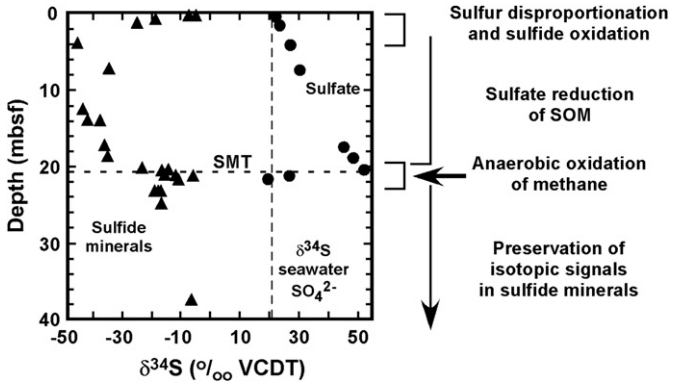

Figure 4. Diagram (using data from Site 995, Table 1, Fig. 2) showing the stratigraphic zonation of dominant sulfur transformations within Blake Ridge and Carolina Rise sediments. From the oxic seafloor to the uppermost sulfate reduction zone, successive steps of reduction and oxidation of sulfur species and sulfur disproportionation drive the sulfur isotopic composition ($\delta^{34}S$) of sulfide minerals (filled triangles) to high depletions in ^{34}S, forming the characteristic background (or baseline) values of −40 to −50‰ CDT found in most continental-margin sediments. In the sulfate reduction zone, the sulfate pool becomes more enriched in ^{34}S (filled circles) with depth as the sulfate reduction occurs, also enriching the dissolved sulfide pool, so that sulfide minerals more enriched in ^{34}S are added to the background signal of $\delta^{34}S$. Thus, bulk sulfide minerals become more enriched in ^{34}S with increasing depth. At the SMT, dissolved sulfate is maximally enriched in ^{34}S so that dissolved sulfide and sulfide minerals produced here are also maximally enriched in ^{34}S. Below the SMT, the $\delta^{34}S$ signal of sulfide minerals is preserved.

counter-intuitively, large enrichments of ^{34}S occur in sulfate even when large amounts of sulfate are depleted by AOM in fully open systems (Jorgensen et al., 2004); that is, $\delta^{34}S_{SO4}$ values can exceed that of seawater sulfate (21‰). This obviously occurs at Sites 994 and 995 ($\delta^{34}S_{SO4}$ values of 49.6‰ and 51.6‰, respectively) of the Blake Ridge (Table 1, Fig. 2) and it occurs elsewhere. For example, Jorgensen et al. (2004) describe the sulfur geochemistry of three cores from the Black Sea that display linear sulfate profiles through the bulk of the sulfate reduction zone. They demonstrate that sulfide mineral precipitation driven by AOM occurs below and at the SMT, where $\delta^{34}S_{SO4}$ ranges from ~48 to 59‰ analogous to Blake Ridge values. These ^{34}S enrichments are transferred from the sulfate pool into the dissolved sulfide pool and then finally into iron sulfide minerals near the SMT. However, peak amounts of sulfide minerals may not occur at the present-day SMT, because sulfide mineralization is a cumulative process. Although the peak in sulfide mineral abundance occurs at the present-day SMT at Site 994, peak sulfide mineral abundance at sites 995 and 11-8 (as well as a secondary peak at Site 994) occurs below the present-day SMT perhaps due to the sustained action of AOM at the SMT in the recent geologic past (see Section 4.3). Increases in sulfide mineral abundance at Sites 994 and 995 are also coincident with localized increases in carbonate weight percent with carbon isotopic signatures indicative of AOM at the SMT (Rodriguez et al., 2000). Because interstitial sulfate is maximally enriched in ^{34}S at the SMT (Fig. 2), transfer of ^{34}S into sulfide mineral phases there results in significant ^{34}S enrichment compared to that of sulfide minerals formed higher in the sulfate reduction zone.

The amount of authigenic sulfide minerals and the relative magnitude of ^{34}S enrichment is dependent on a variety of sedimentological and diagenetic factors including sedimentation rate (Raiswell, 1988), sulfate reduction rates (Canfield et al., 2000; Habicht and Canfield, 2001), AOM rate (in turn dependent on methane delivery to the SMT; e.g., Borowski et al., 1996), and

availability of interstitial iron (Canfield, 1989; Canfield et al., 1992). A case of pronounced sulfide mineralization associated with the SMT and AOM (Schultz et al., 1994; Niewohner et al., 1998) occurs in Amazon fan sediments (Kasten et al., 1998; Adler et al., 2000). A 25–30-cm-thick layer contains up to 8 wt% sulfur comprised of greigite (no pyrite), 80 cm below the SMT. Adler et al. (2000) attribute sulfide mineral precipitation below the SMT to downward diffusion of dissolved hydrogen sulfide where it precipitates due the availability of dissolved iron produced from iron hydroxides. Thus, sulfide minerals enriched in ^{34}S below the Blake Ridge SMTs may be to due to similar conditions or to a stratigraphically static SMT. Because of low amounts of interstitial $\sum HS^-$ and thus no apparent limitation in interstitial iron within Blake Ridge sediments, we infer that zones of ^{34}S-enriched sulfide minerals below the present-day SMT result from comparable diagenetic processes occurring in the recent geologic past that represent "paleo" or "fossil" SMTs (e.g., Dickens, 2001; see Section 4.3).

4.2. Additional controls on pore-water sulfate isotopic composition

The isotopic composition of seawater sulfate has changed markedly since the Precambrian based on ^{34}S measurements of sulfur in evaporites (Claypool et al., 1980), barite (Paytan et al., 1998: Dickens, 2001), and carbonates (Strauss, 1999). The geological range in seawater sulfate $\delta^{34}S$ values is predominantly between +10 and +30‰ CDT (Bottrell and Newton, 2006) so that isotopic signals preserved within sulfide minerals will vary according to their age of formation, in addition to the amount of sulfur mineralization at the SMT. Although the isotopic composition of seawater sulfate is an initial factor, we suggest that it is the *relative* difference between $\delta^{34}S$ values of sulfide minerals (created by AOM near the SMT) to the background $\delta^{34}S$ values created by sulfur disproportionation and other factors that allow recognition of ^{34}S-enriched sulfide mineral layers in the geologic record. The magnitude of this difference will be controlled by the fractionation factor of any sulfur transformations plus a complex interplay between all the aforementioned factors.

4.3. Recognition of "fossil" SMTs

We propose that stratigraphic occurrences of ^{34}S-enriched sulfide minerals is a proxy for identifying the stratigraphic locations of former sulfate–methane transitions (Fig. 5) in a manner analogous to that of authigenic carbonate (e.g., Raiswell, 1988; Rodriguez et al., 2000; Ussler and Paull, 2008) and barite (e.g., Torres et al., 1996; Dickens, 2001) mineralization. Assuming that diagenetic rates for a given depositional environment are relatively constant (e.g., Raiswell, 1988), the interplay among upward methane delivery, accumulation rate, and burial rate will control both the amount of authigenic minerals and their isotopic composition. Hence long-lived and stratigraphically static diagenetic fronts will accumulate more authigenic sulfide minerals possessing an isotopic composition indicative of diagenetic processes occurring near the SMT.

With continued deposition, horizons with accumulations of ^{34}S-enriched sulfide sulfur formed at the SMT will persist and move downward in the sedimentary section, leading to ^{34}S-enriched sediments below the SMT. For example, $\delta^{34}S_{\text{sulfide mineral}}$ data from the Blake Ridge show ^{34}S enrichments below the SMT (Fig. 2, Table 1). For core 11-8, maximal $\delta^{34}S$ sulfide mineral values occur at the SMT, but 2 samples below show positive $\delta^{34}S$ values, whereas at Site 994, 12 samples show higher $\delta^{34}S$ values below the SMT. The lack of ^{34}S enrichments in sulfide minerals above the present-day SMT indicates that the SMT has not moved upward since the equilibration of the observed sulfate profiles (see below).

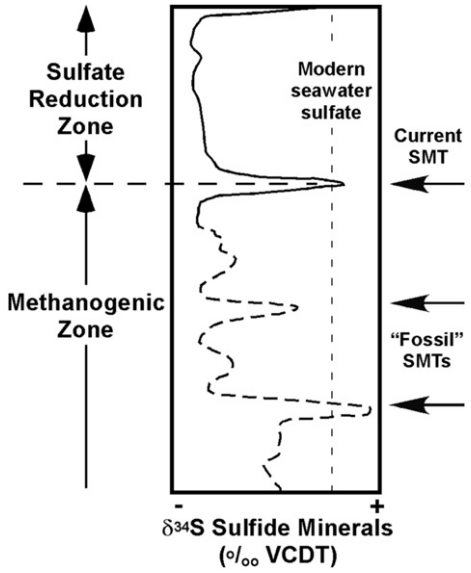

Figure 5. Schematic diagram showing idealized stratigraphic changes in the sulfur isotopic composition ($\delta^{34}S$ CDT) of authigenic sulfide minerals (native sulfur, iron monosulfides, pyrite) in continental rise sediments. $\delta^{34}S$ values near and above the present-day sulfate–methane transition (SMT) zone reflect data from Fig. 2 (solid), whereas the curve below is speculative (dashed). Large depletions of ^{34}S (more negative $\delta^{34}S$ values) indicate mineral formation in the upper sulfate reduction zone; enrichment of ^{34}S (positive excursions of $\delta^{34}S$ values) indicates mineral formation at or near the current SMT (solid arrow), or at past locations (dashed arrows) of the SMT. Under normal conditions, enrichments of ^{34}S occurring near the sediment–water interface are erased by continued sulfur diagenesis with burial, so should be absent or poorly preserved in the geologic record.

4.4. Mass balance estimates of sulfide minerals produced by AOM

We first characterize the sulfur diagenetic system at the Blake Ridge by comparing observed $\delta^{34}S_{SO4}$ values to those predicted by closed and open system behavior (Fig. 6) using equations derived by Canfield (2001). Our sulfide mineral data most closely match open-system conditions, with the sulfur fractionation factor (α) between dissolved sulfate and sulfide being ~1.010 for core 11-8, and ~1.029 for sites 994 and 995.

It is possible to estimate the amount of sulfide minerals produced by AOM using measured $\delta^{34}S_{\text{sulfide mineral}}$ values and a mixing model together with a few basic assumptions (Table 2). For simplicity, the model contains only two end members: those sulfide minerals produced by sulfate reduction and sulfur disproportionation near the top of the sulfate reduction zone, and those produced by AOM at the SMT, although we realize that sulfide minerals can also form throughout the sulfate reduction zone. In the model, the ^{34}S-depleted end-member or background $\delta^{34}S$ value is −46.5‰ (the average of the most negative $\delta^{34}S_{\text{sulfide mineral}}$ values for sites 994 and 995, samples 1H-3, 140–150 cm and 108–118 cm respectively; Table 1). For the ^{34}S-enriched end-member, the $\delta^{34}S_{\text{sulfide mineral}}$ value precipitated at the SMT depends on the local sulfur isotopic value of sulfate being reduced there, consequently we estimate the $\delta^{34}S_{\sum HS^-}$ value using the maximum $\delta^{34}S$ value for sulfate. The model also assumes that there is no fractionation between the dissolved sulfide and sulfide mineral pools. These simplifying assumptions are reasonable because sulfate is essentially quantitatively reduced to $\sum HS^-$ at the SMT, thus retaining the sulfur isotopic signal of that sulfate, and because there is only a small (~1‰) fractionation from dissolved sulfide to sulfide minerals (Price and Shieh, 1979; Wilkin and Barnes, 1996). Each end-member value is then used by the mixing model to estimate the amount of solid-phase sulfide

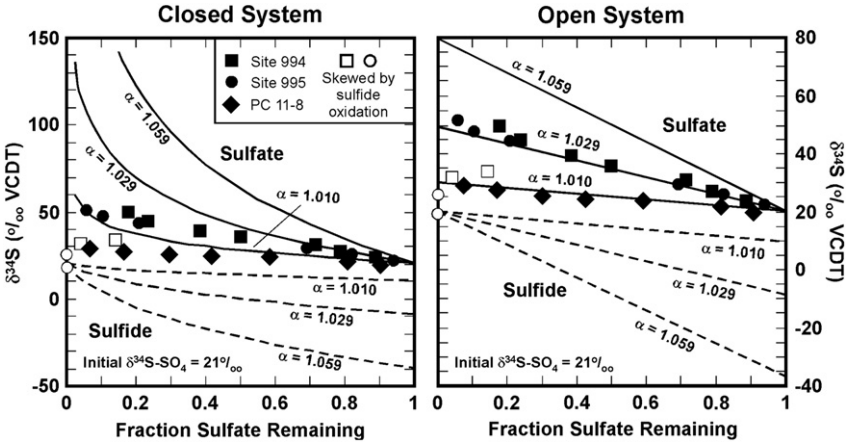

Figure 6. Model fractionation of sulfur isotopes in closed and open systems for the sulfate-sulfide system at various fractionation factors (α); model equations for both systems are given by Canfield (2001). Sulfur isotopic compositions ($\delta^{34}S$) are relative to the Canyon Diablo Troilite (CDT) standard and are given in per mil units (‰). Initial sulfate $\delta^{34}S$ is 21‰. The evolution of $\delta^{34}S$ values of dissolved sulfate is given by the solid lines with corresponding $\delta^{34}S$ values of sulfide shown by dashed lines. Symbols refer to samples taken at Ocean Drilling Programs (ODP) sites 994 and 995, and at piston core site 11-8; all samples are from the Blake Ridge (Borowski et al., 1999). Open symbols refer to those samples that have been affected by sample handling, where dissolved sulfide has been oxidized to sulfate thus skewing their $\delta^{34}S$ values. Note that the samples more closely match the model curves given by the open system. Also, any dissolved sulfide produced near the sulfate–methane transition will likely have a $\delta^{34}S$ value approaching 21‰.

produced by AOM at the SMT for any particular sample tabulated in Table 2. For example for core 11-8 (10.59 mbsf), sulfide minerals produced solely by precipitation at the SMT would possess a $\delta^{34}S$ value of 29.1‰; those sulfide minerals produced only by sulfate reduction and disproportionation would have a $\delta^{34}S$ value of −46.5‰. Using this estimation, we are testing to see if appreciable amounts of the sulfide minerals can be plausibly produced by AOM.

The model estimates that 92%, 20%, and 23%, of sulfide minerals were produced by AOM at the present-day SMT at sites 11-8, 994, and 995, respectively (Table 2). Note also that deeper samples from core 11-8 (11.59 and 12.65 mbsf) and Site 994 (34.89 mbsf) contain appreciable proportions of AOM-formed sulfide minerals, which we interpret to represent stratigraphic locations of "fossil" or "paleo" SMTs. At site 994, evidence for a fossil SMT is further supported by an associated increase of total carbonate and a minimum in the $\delta^{13}C$ values of both calcite and dolomite (Rodriguez et al., 2000).

Another approach in assessing the role of AOM in producing sulfide minerals is to estimate the sulfur isotopic composition of the $\sum HS^-$ pool near the SMT using the fractionation factor between the sulfate and sulfide pools pictured for the open-system case in Figure 6. We apply the respective fractionation factor for each site (Table 2) to the maximum $\delta^{34}S_{SO4}$ values near the SMT (Table 2). For example, for core 11-8, the maximum $\delta^{34}S_{SO4}$ value is 29.1‰ and a fractionation factor (α) of 1.010 yields dissolved sulfide with a $\delta^{34}S$ value of 18.9‰. The model end-members cases (sulfide modified by sulfur disproportionation, −46.5‰; and sulfide formed through AOM, 18.9‰) are mixed together to calculate the proportion of sulfide donated through AOM. For core 11-8 (10.59 mbsf), Site 994

Table 2
Data used in the mass balance model and model calculations predicting the $\delta^{34}S$ values and fraction of sulfide minerals produced at the SMT by anaerobic oxidation of methane. See text for explanation.

Site	SMT depth (m)	Sample depth (m)	Sulfide sulfur (wt%)	$\delta^{34}S$ sulfide minerals[a] (‰ VCDT)	Maximum $\delta^{34}S$-SO_4[b] (‰ VCDT)	Model-predicted sulfurfractionation factor[c] (α)	Fractionation-predicted $\delta^{34}S$-$\sum HS^-$[d] (‰ VCDT)	Proportion of sulfide minerals produced by AOM	
								Maximum $\delta^{34}S$-SO_4[e] (%)	Fractionation-predicted[f] (%)
PC 11-8	10.3	10.59	0.08	23.6	29.1	1.010	18.9	92.7	100.7
		11.59	0.14	5.3				68.5	76.2
		12.65	0.30	3.4				66.0	79.2
994	~20	20.50	0.32	−26.9	49.6	1.029	20.0	20.4	29.5
		20.15[g]	0.44[g]	−29.6[g]				17.6	25.4
		21.80	0.32	−17.7				30.0	43.3
		28.89	0.68	−3.2				45.0	65.1
		34.89	0.42	18.8				68.0	98.2
995	~21	20.40	0.33	−23.5	51.6	1.029	21.9	23.4	33.6
		20.60[h]	0.33[h]	−18.3[h]				28.7	33.6

[a] Selected samples from Table 1.
[b] See Table 1.
[c] Estimated from Figure 6, open system case.
[d] Calculated from maximum $\delta^{34}S$-SO_4 and observed fractionation factor (α).
[e] Proportion of sulfide mineral produced by AOM based on maximum $\delta^{34}S$-SO_4 with no fractionation.
[f] Proportion of sulfide mineral produced by AOM based on fractionation factor.
[g] Average of values from 20.30 to 20.85 mbsf.
[h] Average of values from 20.40 to 20.80 mbsf.

(20.50 mbsf), and Site 995 (20.40 mbsf), the model predicts that 100%, 29%, and 33% of solid-phase sulfide were produced by AOM. Note that the above estimate for core 11-8 exceeds 100%, indicating that the approach likely overestimates the role of AMO. This approach yields estimates that predict a larger role for AOM-related sulfide mineralization (Table 2).

The mixing model provides rough estimates of likely $\delta^{34}S$ values for dissolved sulfide near the SMT with some caveats. Canfield's (2001) model for open-system fractionation (Fig. 6) does not account for sulfate diffusion into the sediments from overlying seawater, which must be a paramount process for enhanced AOM due to balanced sulfate and methane delivery to the SMT for the Blake Ridge sites. There are also indications from the literature (e.g., Jorgensen, 1979: Sim et al., 2011) that the sulfur isotopic fractionation for sulfate to sulfide in both cultures and nature can be as large as ~70‰, equivalent to a fractionation factor of ~1.074. Such large fractionation factors are presently documented in systems with a deep sulfate source under conditions of higher temperature (e.g., Bottrell et al., 2000; Rudnicki et al., 2001; Wortmann et al., 2001), rather than under shallow subsurface conditions with seawater sulfate as a sulfur source. In such extreme cases, the fractionation factor shown in Figure 6 and used in our mixing model would be underestimated.

Nonetheless, the mixing model shows that samples with greater ^{34}S enrichments reflect a greater role for sulfide mineralization through AOM. The key factor is quantitative depletion of porewater sulfate within the SMT that allows large ^{34}S enrichments to occur within sulfide minerals. Recall that low concentrations of dissolved sulfide (<6 μm, Fig. 3) are typically found in Blake Ridge sediments providing strong evidence for quantitative precipitation of sulfide within the SMT. This exercise also demonstrates that even though AOM is a significant process at each site, $\delta^{34}S_{\text{sulfide minerals}}$ may not always show positive values of ^{34}S enrichment, suggesting that other diagenetic factors are involved. For example, larger accumulations of sulfide minerals with greater ^{34}S enrichments are related to the interplay of burial rates and the mobility of the SMT as determined by changing methane flux over geologic time.

4.5. Non-steady-state processes and methane flux

Anomalous accumulations of sulfide minerals at the SMT with large enrichments in ^{34}S likely require non-steady-state conditions. When sediment accumulation and burial rates are equal and upward methane flux is invariant, the SMT will remain at constant depth below the seafloor. Accordingly, a parcel of sediment will continually move downward in the sediment column passing through the SMT. The sediment parcel will acquire additional sulfide minerals at the SMT that are maximally enriched in ^{34}S, but the contribution of ^{34}S-enrichment will be more-or-less equally distributed ("smeared") throughout the sediment column and the characteristic signal of AOM taking place at the transition will be poorly preserved.

Under non-steady-state conditions, methane flux could control the pace of AOM and thus the accumulation rate and isotopic composition of authigenic sulfide minerals. Table 3 shows sulfate flux calculated from linear sulfate profiles (core 11-8; Borowski et al., 1996) or from diagenetic modeling (ODP Sites 994 and 995; Dickens, 2001). Using the measured amounts of sulfide sulfur in selected sediment samples (Table 1), we calculate the mass of sulfide sulfur in 1 cm^3 of wet sediment and divide it by the corresponding flux of sulfate (=sulfur) to the sulfate–methane interface to obtain the time necessary to accumulate sulfide sulfur. The calculation assumes sediment porosity of 0.70 (Dickens, 2001), sediment density of 2.7 g cm^{-3}, complete conversion of sulfate to dissolved sulfide at the SMT, quantitative precipitation of sulfide minerals, and sulfide mineralization focused within a depth interval of 10 cm. Using these assumptions, it takes on the order of 10^2 to 10^3 years to produce the observed amount of sulfide minerals. Thus it is possible to accumulate the observed amounts of sulfide minerals using AOM-generated sulfide given the sediment ages at the SMT (>50 ky for site 11-8, Borowski, 1998; and >460 ky for the ODP sites, Okada, 2000). These time estimates for sulfide mineralization are similar to that for authigenic carbonate formation (~5900 y) associated with AOM in methane-rich sediments of the Gulf of Mexico (Ussler and Paull, 2008).

Barite also precipitates at the SMT within Blake Ridge sediments but at different rates than that for sulfide mineralization. Snyder et al. (2007b) estimate that barite mineral precipitation at Sites 994 and 995 took at least 45 ky (and perhaps much longer) – a time estimate much longer than ours for sulfide mineral precipitation. There are several reasons for the disparity in mineral accumulation time for iron sulfide versus barite. First, the rate of barite mineral formation is dependent on the delivery rate of dissolved barium from below the SMT (Dickens, 2001; Snyder et al., 2007b). Sulfate

Table 3
Table of sample sites and selected samples showing pertinent sulfur data along with estimated sulfate flux and the time necessary to produce observed sulfide mineral concentrations for each selected sample.

Site	SMT depth (m)	Sample depth (mbsf)	Sulfide sulfur (wt%)	Sulfide sulfur[a] (g)	Sulfide sulfur (10^{-5} mol)	Sulfate flux[b] (mole m^{-2} ky^{-1})	Time necessary to produce observed sulfide amount[c] (years)
PC 11-8	10.3	9.61	0.08	0.0006	1.9	16.2[d]	117
		11.59	0.14	0.0011	3.4		210
		12.65	0.30	0.0024	7.5		463
994	~21	20.50	0.32	0.0026	8.1	7.9[e]	1025
		20.48[f]	0.44[f]	0.0036	11.2		1418
		21.80	0.32	0.0026	8.1		1025
		28.89	0.68	0.0055	17.2		2177
		34.89	0.42	0.0034	10.6		1342
995	~21	20.40	0.33	0.0027	8.4	7.6[e]	1105
		20.60[g]	0.33[g]	0.0027	8.4		1105
		21.42	0.44	0.0036	11.2		1474

[a] Mass per 1 cm^3 wet sediment; average sediment porosity = 0.3; average sediment density = 2.7 g cm^{-3}.
[b] At the sulfate–methane transition, assume sulfate flux = sulfide production.
[c] Based on sulfide mineral accumulation layer 10 cm thick; sample interval of ODP samples.
[d] From Borowski et al. (1996), decreased by 10% according to Dickens (2001).
[e] From Dickens (2001).
[f] Average of values from 20.30 to 20.85 mbsf.
[g] Average of values from 20.40 to 20.80 mbsf.

concentrations (millimolar, mM, levels) and fluxes (7.9 and 7.1 mmol m^{-2} ky^{-1} for sites 994 and 995, respectively) exceed those of barite (<1–57 micromolar, μM; 0.044 and 0.015 mmol m^{-2} ky^{-1} for sites 994 and 995, respectively) by over 2 orders of magnitude. Barium flux is independent of the magnitude of sulfate and methane flux (Snyder et al., 2007b), so barite precipitation occurs more slowly. Second, our calculations for sulfide mineral formation assume precipitation in a single, short depth interval of 10 cm, whereas the total interval of sulfide precipitation is potentially much broader. This brings up an interesting point in the pattern of sulfide mineral accumulation that illustrates non-steady-state conditions.

Given that AOM is a major sulfate depletion pathway in methane-rich sediments, a change in methane flux will affect the downward sulfate diffusion rate and the depth of the SMT (Borowski et al., 1996; Dickens, 2001). We postulate that the upward movement of the SMT is in part responsible for ^{34}S enrichments below the present-day SMT where AOM occurred over the recent past. Above (Section 4.3), we stress that occurrences of ^{34}S-enriched sulfide minerals can represent former levels of the SMT but such enrichments can also record movements of the SMT from one relatively long-lived sediment position to another. Some of the ^{34}S-enriched sulfide mineral accumulations observed within Blake Ridge sediments may also represent sulfide precipitation occurring as increased methane flux forces the SMT higher in the sediment column. In other words, the new SMT may have only just arrived at its present depth with the pore-water profiles barely in equilibrium with present, upward methane flux so that more sulfide mineralization may be expected below the SMT rather than at it (Fig. 2, sites 994 and 995). As the sulfate profile moves toward equilibration with higher upward methane flux (Dickens, 2001), the interface sweeps upward and sulfide minerals are precipitated in the zone between the former and present-day SMTs. Dickens (2001) has shown with transient modeling that an upward shift of the SMT at the Blake Ridge from 20 mbsf (seen presently at Sites 994 and 995) to 10 mbsf would fully equilibrate in about 20 ky. A better estimate of sulfide mineral accumulation time would thus include the depth-integrated amount of sulfide minerals between the former and present positions of the SMT, and significantly increase the sulfide mineral accumulation time to become more congruent with time estimates of barite precipitation. Unfortunately, there is no age information contained within authigenic sulfide mineral accumulations other than they must be younger than their host sediments. Without age information we cannot locate the depth of the former SMT and cannot provide an improved time estimate for integrated sulfide mineral precipitation. However, relying on the transient modeling by Dickens (2001), we envision this SMT movement and accompanying sulfide mineralization occurring as a result of increasing methane flux over a minimum time of 10^4 years.

4.6. Recognition of ancient methane-rich sediments and gas hydrates

Layers of sulfide minerals enriched in ^{34}S point to the co-action of sulfate reducers and *Archaea* and significant amounts of interstitial sulfate depletion through AOM. A necessary component of a deep-water, continental-system system with AOM as an important diagenetic process is sufficient methane delivery to the SMT (Borowski et al., 1996, 1997, 1999, 2000). Thus, enrichments of ^{34}S in sulfide minerals are a potential proxy for the occurrence of methane-rich pore waters in the geological past. Moreover, given cold bottom-water temperatures and adequate water depth (i.e., pressure) ^{34}S enrichments in sulfide minerals may help identify former gas hydrate terranes.

4.7. Corroboratory evidence

Significant amounts of sulfate depletion by AOM have other consequences that could be preserved as geochemical signals within the sediment and rock record. Co-occurrence of positive $\delta^{34}S_{\text{sulfide mineral}}$ values together with other indicators of AOM thus strengthens attribution to AOM. Local peaks in alkalinity often co-occur with AOM (e.g., Schultz et al., 1994; Fig. 1) and thus form a diagenetic environment conducive to calcium carbonate precipitation. Widespread authigenic carbonate precipitation is well known at methane seeps (e.g., Naehr et al., 2000) where high rates of AOM occur, but also occurs under diffusive conditions within Blake Ridge sediments (Rodriguez et al., 2000) and elsewhere (Ussler and Paull, 2008). The interstitial, dissolved $\sum CO_2$ pool produced at the SMT by AOM has significant amounts of methane-derived-carbon and is thus strongly depleted in ^{13}C (e.g., Reeburgh, 1976, 1983; Borowski et al., 1997; Fig. 1). As a result, authigenic carbonates forming in SMT zones by AOM will have diagnostic, ^{13}C-depleted isotopic signatures (e.g., Blake Ridge, Rodriguez et al., 2000; Gulf of Mexico, Ussler and Paull, 2008).

The microbial consortium mediating AOM also produces distinctive biomarkers that are potentially preserved within the sediment record. Archeal biomarkers such as glycerol dialkyl glycerol tetraether have been linked to AOM (Pancost et al., 2001), and specific phospholipid fatty acids identify the presence of sulfate reducers in the AOM consortium (Thiel et al., 2001; Zhang et al., 2002). These compounds have been detected in the rock record; for example, Thiel et al. (2001) discovered ^{13}C-depleted crocetane and pentamethylicosane in an Oligocene seep carbonate. Biomarkers associated with AOM have not been measured in Blake Ridge sediments, nor at other diffusive sites with AOM as an important sulfate-depletion mechanism. Although the studies cited above are from advective environments where AOM rates are comparatively high and presumably production of biomarkers is also high so that their preservation is more likely, this should not preclude attempts to measure AOM-associated biomarkers within gas hydrate terranes.

4.8. Global patterns of ^{34}S enrichment

To test the relationship between ^{34}S enrichments of sulfide minerals and AOM, we compiled data for the sulfur isotopic composition of sulfide minerals from the literature to discover patterns of heavy sulfur enrichment in modern sedimentary environments (Table S1, Fig. 7). The data are from a wide variety of depositional environments: lakes (saline and freshwater), coastal (estuary, salt marsh, tidal flat, fjords), oceanic (silled basins, offshore basin, continental rise, ridge crest, cold seep) that also include gas hydrate terranes (Blake Ridge, Cascadia), brine pools (Tyro Basin), euxinic basins (Caricao, Black Sea), and shallow seas (Baltic and Marmara). Hydrothermal or non-sedimentary sulfide deposits are not included in the data set. Researchers extracted various phases of sulfur from sulfide minerals that include acid volatile sulfur (AVS, typically assumed to represent iron monosulfides), pyrite, total sulfur (TS), and total reduced sulfur (TRS) or total reduced inorganic sulfur (TRIS). The data set predominantly includes sulfide extractions that either capture sulfide phases separately with sequential extractions (Zhabina and Volkov, 1978), or capture bulk sulfide minerals (TRS, TRIS) via chromium reduction (Canfield et al., 1986). $\delta^{34}S$ values from elemental sulfur are not tabulated nor included in the histograms.

A histogram of all isotopic measurements ($N = 2504$) mostly shows negative $\delta^{34}S$ values (Fig. 7A) broadly consistent with the sulfur isotopic composition of later Cenozoic, seawater sulfate ($\delta^{34}S$ ranging from 17 to 23‰; Claypool et al., 1980; Paytan et al., 1998),

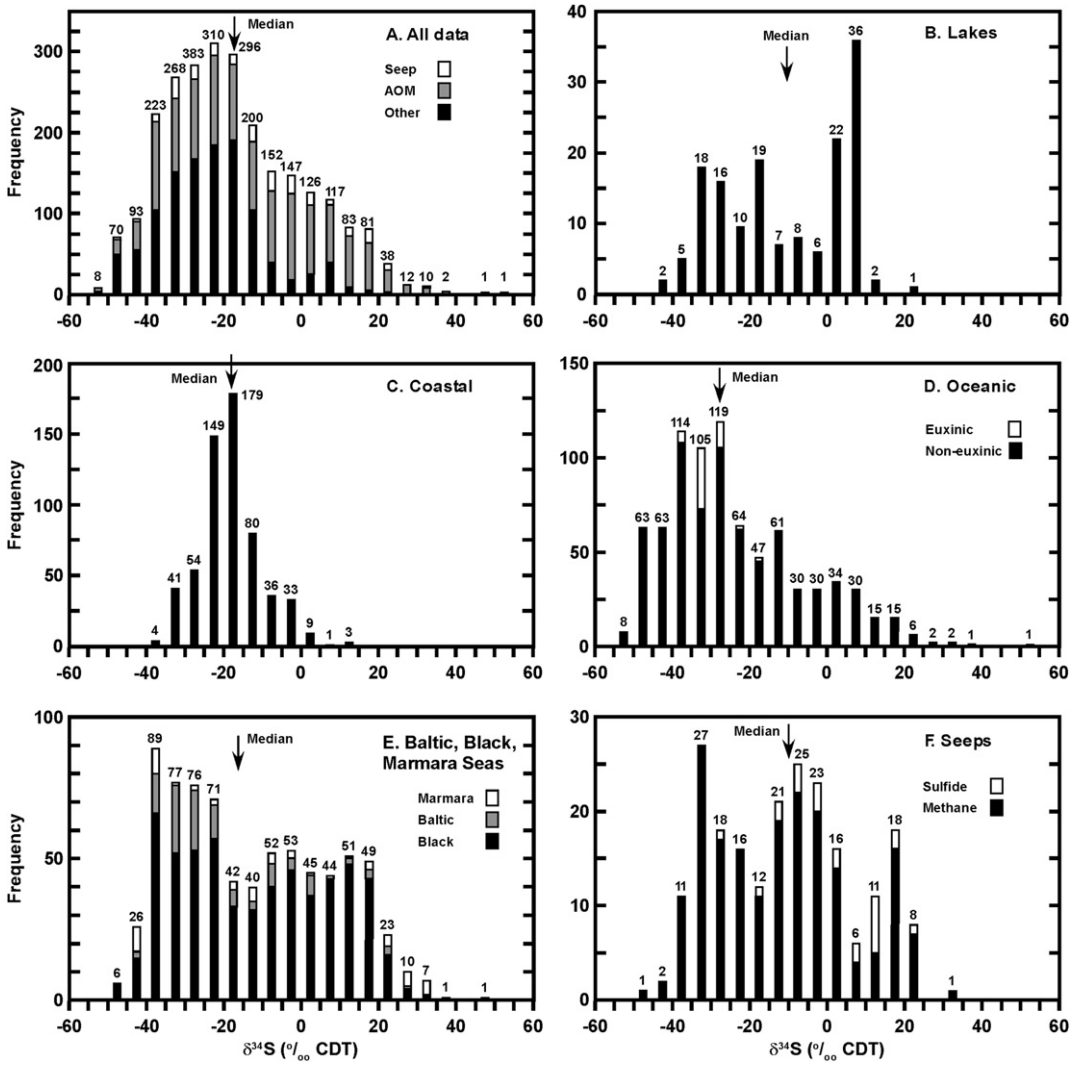

Figure 7. Histograms displaying $\delta^{34}S$ data (per mil, ‰; relative to Canyon Diablo Troilite, CDT) from various phases of sedimentary sulfide minerals (see text and Supplemental section for explanations and data). Values for $\delta^{34}S$ are separated into bins representing 5‰ spanning values from −60‰ to +60‰. Each measurement represents a data point in the histogram; context for the data in the form of an abbreviated spreadsheet appears in Table S1, available in the supplementary section. Histogram A displays all available data ($N = 2504$), but does distinguish between seep sites (white) and sites where anaerobic oxidation of methane (AOM) is a key diagenetic process, from the remainder of the data (black). Data from lakes and coastal environments are shown in histograms B and C, respectively. Histogram D illustrates data from oceanic settings, and distinguishes between sediments with overlying oxygenated water (non-euxinic) and oxygen-free water (euxinic). Data from the Black, Baltic, and Marmara seas appear in histogram E; histogram F shows data from both sulfide and methane seafloor seeps.

and the fractionation inherent in microbial sulfate reduction (~−8 to −40‰; Chambers and Trudinger, 1978). Mean and median values for $\delta^{34}S_{\text{sulfide minerals}}$ are −17 ± 17.4‰ and −19.5‰, respectively (Table 4). The distribution is not Gaussian, but is rather skewed toward positive $\delta^{34}S$ values, which comprise 18.5% (464 instances) of the total data set (Table 4). The majority of positive $\delta^{34}S$ values are associated with significant AOM activity, including that occurring within gas hydrate terranes, followed by seep (Fig. 7F) and shallow-sea (Fig. 7E) occurrences, respectively.

Lake environments include data ($N = 152$) from both freshwater and saline lakes (Fig. 7B). $\delta^{34}S$ values (mean = −10.7 ± 15.9‰, median = −10.5‰; Table 4) are mostly negative (~60%, 91 of 152

Table 4
Statistical parameters for $\delta^{34}S$ values of sulfide minerals from the literature arranged by environmental setting.

Geologic setting	*N*	$\delta^{34}S$ – sulfide minerals (‰, CDT)				
		Range		Standard		
		Low	High	Mean	Deviation	Median
All	2530	−54.1	53	−17	18	−20
Lakes	152	−41	9.4	−11	16	−11
Coastal	589	−38	11	−18	8	−19
Oceanic	810	−54.1	53	−24	18	−28
Seas	763	−40	45.5	−13	20	−16
Seeps	216	−47.9	32	−11	18	−10

values) with a considerable number of positive values. Most positive values are from a series of lakes in northern Ontario affected by acid rain and associated sulfur deposition (55 values; Table S1) or from saline lakes of the Lake Chany complex in Siberia (4 data points; Table S1). Freshwater lakes with more typical natural processes or other saline lakes (e.g., Owens Lake, California) have $\delta^{34}S$ values that are strongly negative (Table S1).

Coastal environments ($N = 589$) span a very diverse range of settings and show sulfide isotopic data that are strongly negative (mean $= -18 \pm 8.1‰$, median $= -18.8‰$; Fig. 7C; Table 4). Positive $\delta^{34}S$ values are few (13, or 2%) and occur only at Cape Lookout Bight, North Carolina (9 values, Table S1) and Krossfjorden at Svalbard (4 values, Table S1).

Ocean environments display diverse settings include euxinic and non-euxinic conditions and gas hydrate terranes (Fig. 7D; Table 4), as well as shallow seas (Fig. 7E; Table 4) and advective sites (cold seeps; Fig. 7F; Table 4), which are tabulated separately. Data from oceanic localities (Fig. 7D) show dominantly negative $\delta^{34}S$ values (784 values, or 87%; mean $= -23.6 \pm 17.5‰$, median $= -28‰$) with a wispy tail toward positive values. Measurements from euxinic sediments (e.g., Cariaco Basin) show no positive $\delta^{34}S$ values (Fig. 7D); any positive values are from sediments with oxygenated overlying waters. The bulk of the positive $\delta^{34}S$ values are found at offshore Namibia under the Benguela Current (39 instances, $\delta^{34}S = 0$ to 13‰; Table S1) and within gas hydrate terranes of Cascadia (40 instances, $\delta^{34}S = 2$ to 53‰; Table S1) and the Blake Ridge (4 instances, 3–23‰; Table S1).

The Baltic, Black, and Marmara seas have a similar sedimentary history but only the Black Sea is euxinic over a portion of its extent. The distribution of $\delta^{34}S$ values for sedimentary sulfide minerals is more evenly distributed over the range of possible values (mean $= -12.5 \pm 20.2‰$, median $= -16‰$; Fig. 7E; Table 4), and contains many more positive $\delta^{34}S$ values (231 instances, or 30%) compared to other environments. Because measurements from Black Sea sediments are much more numerous, more positive $\delta^{34}S$ values are recorded there. Data from the euxinic portions of the Black Sea (Fig. 7D) are distributed throughout the range of $\delta^{34}S$ values, suggesting that the oxygen content of the water overlying sediments is not a factor controlling the positive $\delta^{34}S$ value occurrences.

Cold seeps leak a combination of methane and sulfide into overlying seawater, and both seep types display a range of $\delta^{34}S$ values (Fig. 7F; Table S1). Cold seep environments display proportionately more positive $\delta^{34}S$ values (mean $= -10.5 \pm 18‰$, median $= -10‰$), which comprise 27.8% of measurements (60 of 216). ^{34}S enrichments in the case of sulfide-rich seeps of the Florida escarpment are indicative of the source of sulfide sulfur within the carbonate massif (Commeau et al., 1987; Paull and Neumann, 1987; Chanton et al., 1993). Methane seeps are usually sulfide-rich because higher concentrations of sulfate sulfur sourced from overlying seawater come into contact with methane. Advection of methane fuels AOM as seawater sulfate is converted to sulfide that precipitates and often shows ^{34}S enrichment.

Data from the literature show that heavy sulfide mineralization occurs commensurate with significant levels of AOM under several scenarios (Table 5 and Table S1). About 49.8% of the measurements (234 of 471) show ^{34}S enrichments when marine sediments overlie a potent dissolved-iron source in the form of freshwater sediments (i.e., the Baltic, Black, and Marmara Seas). Bottcher and Lepland (2000) and Jorgensen et al. (2004) clearly demonstrate that dissolved iron diffusing upward from underlying freshwater sediments precipitates as iron sulfide minerals when encountering a downward-diffusing sulfide front created largely by AOM. They emphasize that the excess source of iron from below limits sulfide diffusion away from the SMT to form sharply defined concentrations of sulfide minerals enriched in ^{34}S. Freshwater sediments also exist below marine sediments in Kau Bay where Middleburg (1991) document ^{34}S enrichments and recognize the role of dissolved iron availability and downward sulfide diffusion. Severe organic carbon loading at Cape Lookout Bight creates dual production of biogenic methane and sulfide through sulfate reduction that results in ^{34}S-enriched sulfide minerals (Chanton et al., 1987). At offshore Namibia (Dale et al., 2009), a distinct diffusion profile of dissolved sulfide is clearly produced at the SMT where dissolved sulfate and sulfide are maximally enriched in ^{34}S at the SMT. Pyrite is also enriched near the SMT (up to 5.3‰) with larger enrichments (up to 13‰) occurring below.

The only other gas hydrate terrane where $\delta^{34}S_{\text{sulfide minerals}}$ data exist is at Cascadia (Table 5 and Table S1). However, these samples from offshore Vancouver Island (ODP Leg 141, IODP Leg 311) are predominantly from well below present-day SMTs. Some ^{34}S enrichments may be associated with present-day AOM (Site 888, 1 sample; Site 889/890, 1 sample, Bottrell et al., 2000; Site 1329, 1 sample, Wang et al., 2008) but the data are equivocal.

Not counting seep cases, approximately 80% of the measurements displaying ^{34}S enrichments (331 of 412) can be interpreted as being related to AOM at the SMT. Jorgensen et al. (2004) emphasize that AOM is replete in marine sediments and special conditions such as those discussed above enable enrichments of ^{34}S in sulfide minerals. Because sulfide minerals generally contain distinctly negative $\delta^{34}S$ values as the histogram data demonstrate (Fig. 7), the sulfur isotopic composition of bulk sulfide minerals tends to remain negative even as heavier sulfide sulfur is added to the sediment with burial through the sulfate reduction and AOM zones. Thus, even as sediment experiences AOM as it passes through the SMT during burial, ^{34}S enrichments might not be recognizable in the isotopic signal of sulfide minerals unless large amounts of ^{34}S-enriched minerals are added to the sediment. Most often (~50%) this occurs because of ample sources of dissolved iron from underlying freshwater sediments (Baltic, Black and Marmara Sea, Kau Bay), but also plausibly when AOM as a sulfate depletion mechanism rivals sulfate reduction of SOM (e.g., the Blake Ridge).

4.9. Application to the geologic record

The global sulfur isotopic data show that ^{34}S-enriched sulfide minerals are not unique to localities with AOM as a significant diagenetic process. Nonetheless, the data show that AOM is the most significant causal factor (Table 5) in generating the diagenetic signal at shallow seas or bays that have been inundated by the ocean during the last sea level rise (the Baltic, Black, and Marmara seas; Kau Bay, Indonesia), at seep sites, and at the Blake Ridge. In deeper water, marine environments, methane flux is also related to the presence of underlying gas hydrates (e.g. Borowski et al., 1999). Our preliminary $\delta^{34}S_{\text{sulfide mineral}}$ data from the Blake Ridge region show that it is plausible that gas hydrate terranes will record these signals, linking ^{34}S enrichments of sulfide minerals to gas hydrate occurrence.

Given the diagenetic environments where we find ^{34}S enrichments, it should be straight forward to distinguish gas hydrate environments from most other occurrences. Most ^{34}S enrichments occur where underlying fresh-water sediment provides an excess source of iron to interstitial waters, so that freshwater versus marine sediments should be distinguishable in the geologic record. Seep sites are also favored locations for sulfur isotopic enrichments and their commonly massive occurrences authigenic carbonate formation should be distinctive from marine sediments where diffusive processes dominate. Lastly, some coastal and shallow-water environments have some ^{34}S enrichments, but sediments with underlying gas hydrates should be from slope and deep-water depositional environments. Moreover, corroborative evidence in

Table 5
Summary of occurrences that show consistent ^{34}S enrichments ($\delta^{34}S > 0$) in sulfide minerals. See Table S1 (supplementary materials) for entire data set.

Setting	Location	Circumstance	δ^{34}S-sulfide minerals (‰ CDT)				Reference
			Range			AOM involved	
			N	Low	High		
Freshwater	Connecticut	Ponds	2	1.6	4.6	No	Nakai and Jensen (1964)
Freshwater	Ontario	Sulfur polluted lakes	56	0.2	9.4	No	Nriagu and Coker (1983)
Saline lake	Lake Chany complex West Siberia	Bolson	4	6	21	No	Doi et al. (2004)
Coastal	Cape Lookout Bight	Estuary, organic loading	9	0.6	4.9	Yes	Chanton (1985)
Coastal	Svalbard Krossfjorden (sta. G)	Silled basin	4	6	11	No	Bruchert et al. (2001)
Oceanic	Sanica Monica basin San Diego Trough	Highly reduced sediments, oxidized sediments	3	0.3	4.8	No	Kaplan et al. (1963)
Neretic	Kau Bay, Halmahera, Indonesia	Freshwater sediment	3	4	16	Yes	Middleburg (1991)
Oceanic	Mediterranean	Downward sulfide diff.	7	6	19	No	Passier et al. (1996)
Oceanic	offshore Namibia Benguela	Biotic sulfide oxidation, seasonal anoxia	39	0.03	13	Yes	Dale et al. (2009)
Oceanic	Cascadia Margin	Gas hydrate	40	2	53	Likely	Bottrell et al. (2000), Wang et al. (2008)
Oceanic	Arabian Sea	Western Indus Fan	5	9	15	No	Bottcher et al. (2000a,b)
Oceanic	offshore New Zealand ODP Leg 181	Continental slope	1	9	9	Likely	Bottcher et al. (2004a,b)
Oceanic	Amazon Fan	AOM	4	1.41	34.95	Yes	Bottcher, Schultz et al. (unpublished data)
Oceanic	Blake Ridge	Gas hydrate	4	3.4	23.6	Yes	This paper
Oceanic	Baltic Sea	Freshwater sediment, downward sulfide diffusion	16	1	28	Yes	Sternbeck and Sohlenius (1997), Bottcher and Lepland (2000)
Oceanic	Black Sea	Freshwater sediment, downward sulfide diffusion	194	0.23	45.5	Yes	Various, see Table S1.
	Marmara	Freshwater sediment, downward sulfide diffusion	21	4	38	Yes	Bottcher et al. (unpublished data)
Seep (sulfide)	Florida Escarpment	Advective	12	2	20.8	–	Commeau et al. (1987), Chanton et al. (1993)
Seep (methane)	Hydrate Ridge	Advective	26	0.2	20.3	–	Bottcher et al. (unpublished data)
Seep (methane)	Cascadia Margin	Advective	19	1	32	–	Wang et al. (2008)
Seep (methane)	Monterey Bay	Advective	2	0.46	0.74	–	Paull et al. (unpublished data)
Total			471				

the form of authigenic carbonates (Rodriguez et al., 2000) and archeal biomarkers (e.g., Pancost et al., 2001; Thiel et al., 2001) in deep-water sediments found together with ^{34}S-enriched iron sulfides can strengthen the possibility of the recognition of paleo-SMTs in the sediment and rock record.

5. Summary

Anaerobic oxidation of methane at the base of the sulfate reduction zone (the sulfate–methane transition, SMT) creates a diagenetic environment favorable for the focused formation of authigenic sulfide minerals (So, FeS, FeS_2). At the gas hydrate terrane of the Blake Ridge, these sulfide minerals are enriched in ^{34}S by at least 20‰ CDT on average compared to background $\delta^{34}S$ levels of −40 to −50‰. Larger ^{34}S enrichments imply larger amounts of sulfide minerals precipitated at the SMT as shown by mass balance calculations. These horizons may be proxies for AOM in the geologic record because in deep-water, continental margin environments with less organic loading, AOM becomes a significant sulfate sink due to the increased upward flux of methane in equilibrium with underlying gas hydrates (Borowski et al., 1999). The largest enrichments in ^{34}S should occur under non-steady-state conditions where AOM operates at the same horizon in the sedimentary column for appreciable lengths of geologic time.

Data gathered worldwide from modern and Cenozoic sediments further support a link between AOM and localized enrichments of ^{34}S within sulfide minerals. Although distinctly positive $\delta^{34}S$ values (>0‰ CDT) within sediments are not necessarily diagnostic of significant AOM, the bulk (70%) of such enrichments are associated with AOM. Most observed ^{34}S-enriched sulfide mineral occurrences occur outside of gas hydrate provinces because of sampling frequency artifacts. To use ^{34}S enrichments as an AOM and gas hydrate indicator for the geologic record, other likely settings must first be eliminated as possibilities, and corroboratory evidence in the form of authigenic carbonate minerals that possess light $\delta^{13}C$ values and/or biomarkers suggestive of the AOM consortium, should be present. The relationship between ^{34}S enrichments of authigenic sulfide minerals, AOM, and gas hydrates must be explored further, particularly in gas hydrate provinces, to firmly establish the utility of $\delta^{34}S_{\text{sulfide minerals}}$ values as a proxy for methane-rich and/or gas-hydrate-bearing sediments.

Acknowledgments

We thank the captains and crew of the *R/V Cape Hatteras* and JOIDES *Resolution*. Many thanks for exceptional collegiality by M. Bottcher, V. Bruchert, and B.B. Jorgensen, who kindly supplied $\delta^{34}S$ data. Comments by S. Bottrell and anonymous reviewers significantly improved the manuscript. Funding was provided by the NSF, DOE-NIGEC, USGS, JOI-USSSP in conjunction with the Ocean Drilling Program, Sigma Xi Grants-in-Aid of Research, and the Graduate School of The University of North Carolina, Chapel Hill.

Appendix A. Supplementary material

Supplementary material associated with this article can be found, in the online version, at http://dx.doi.org/10.1016/j.marpetgeo.2012.12.009.

References

Adler, M., Hensen, C., Kasten, S., Schultz, H.D., 2000. Computer simulation of deep sulfate reduction in sediments of the Amazon Fan. International Journal of Earth Sciences 88, 641–654.

Aller, R.C., Rude, P.D., 1988. Complete oxidation of solid phase sulfides by manganese and bacteria in anoxic marine sediments. Geochimica et Cosmochimica Acta 52, 751–765.

Alperin, M.J., Reeburgh, W.S., Whiticar, M.J., 1988. Carbon and hydrogen isotope fractionation resulting from anaerobic methane oxidation. Global Biogeochemical Cycles 2, 279–288.

Berner, R.A., 1964a. Iron sulfides from aqueous solution at low temperatures and atmospheric pressure. Journal of Geology 72, 293–306.

Berner, R.A., 1964b. Stability field of iron minerals in anaerobic marine sediments. Journal of Geology 72, 826–834.

Berner, R.A., 1967. Thermodynamic stability of sedimentary iron sulfides. American Journal of Science 265, 773–785.

Berner, R.A., 1970. Sedimentary pyrite formation. American Journal of Science 268, 1–23.

Bhatmagar, G., Chapman, W.G., Dickens, G.R., Dugan, B., Hirasaki, G.J., 2008. Sulfate–methane transition as a proxy for average methane hydrate saturation in marine sediments. Geophysical Research Letters 35, L03611. http://dx.doi.org/10.1029/2007GL032500.

Borowski, W.S., 1998. Pore water sulfate concentration gradients, isotopic compositions, and diagenetic processes overlying continental margin, methane-rich sediments associated with gas hydrates. Ph.D. dissertation, University of North Carolina, Chapel Hill, North Carolina, USA.

Borowski, W.S., Paull, C.K., Ussler III, W., 1996. Marine pore water sulfate profiles indicate *in situ* methane flux from underlying gas hydrate. Geology 24, 655–658.

Borowski, W.S., Paull, C.K., Ussler III, W., 1997. Carbon cycling within the upper methanogenic zone of continental-rise sediments: an example from the methane-rich sediments overlying the Blake Ridge gas hydrate deposits. Marine Chemistry 57, 299–311.

Borowski, W.S., Paull, C.K., Ussler III, W., 1999. Global and local variations of interstitial sulfate gradients in deep-water, continental margin sediments: sensitivity to underlying methane and gas hydrates. Marine Geology 159, 131–154.

Borowski, W.S., Hoehler, T.M., Alperin, M.J., Rodriguez, N.M., Paull, C.K., 2000. Significance of anaerobic methane oxidation in methane-rich sediments overlying the Blake Ridge gas hydrates. In: Paull, Matsumoto, R., Wallace, P.J., Dillon, W.P. (Eds.), Gas Hydrate Sampling on the Blake Ridge and Carolina Rise. Proceedings ODP, Scientific Results, vol. 164, pp. 87–99. College Station, TX.

Bottcher, M.E., Lepland, A., 2000. Biogeochemistry of sulfur in a sediment core from the west-central Baltic Sea: evidence from stable isotopes and pyrite textures. Journal of Marine Systems 25, 299–312.

Bottcher, M.E., Hespenheide, B., Llobet-Brossa, E., Beardsley, C., Larsen, O., Schramm, A., Wieland, A., Bottcher, G., Berninger, U.G., Amann, R., 2000a. The biogeochemistry, stable isotope geochemistry, and microbial community structure of a temperate intertidal mudflat: an integrated study. Continental Shelf Research 20, 1749–1769.

Bottcher, M.E., Schale, H., Schnetger, B., Wallmann, K., Brumsack, H.J., 2000b. Stable sulfur isotopes indicate net sulfate reduction in near-surface sediments of the deep Arabian Sea. Deep-Sea Research II 47, 2769–2783.

Bottcher, M.E., Hespenheide, B., Brumsack, H.J., Bosselmann, K., 2004a. Stable isotope biogeochemistry of the sulfur cycle in modern marine sediments: I. Seasonal dynamics in a temperate intertidal sandy surface sediment. Isotopes in Environmental and Health Studies 40 (4), 267–283.

Bottcher, M.E., Khim, B.K., Suzuki, A., Gehre, M., Wortmann, U.G., Brumsack, H.J., 2004b. Microbial sulfate reduction in deep sediments of the Southwest Pacific (ODP Leg 181, Sites 111-9-1125): evidence from stable sulfur isotope fractionation and pore water modeling. Marine Geology 205, 249–260.

Bottrell, S.H., Newton, R.J., 2006. Reconstruction of changes in global sulfur cycling from marine sulfate isotopes. Earth-Science Reviews 75, 59–83.

Bottrell, S.H., Parkes, R.J., Cragg, B.A., Raiswell, R., 2000. Isotopic evidence for anoxic pyrite oxidation and stimulation of bacterial sulphate reduction in marine sediments. Journal of the Geological Society, London 157, 711–714.

Bottrell, S.H., Mortimer, R.J.G., Davies, I.N., Harvey, S.M., Krom, M.D., 2009. Sulphur cycling in organic-rich marine sediments from a Scottish fjord. Sedimentology 56, 1159–1173.

Bruchert, V., Knoblauch, C., Jorgensen, B.N., 2001. Controls on stable isotope fractionation during bacterial sulfate reduction in Arctic sediments. Geochimica et Cosmochimica Acta 65 (5), 763–776.

Canfield, D.E., 1989. Reactive iron in marine sediments. Geochimica et Cosmochimica Acta 53, 619–632.

Canfield, D.E., 2001. Biogeochemistry of sulfur isotopes. In: Valley, J.W., Cole, D.R. (Eds.), Stable Isotope Geochemistry. Reviews in Mineralogy and Geochemistry, vol. 43, pp. 607–636.

Canfield, D.E., Thamdrup, B., 1994. The production of ^{34}S-depleted sulfide during bacterial disproportionation of elemental sulfur: Science 266, 1973–1975.

Canfield, D.E., Raiswell, R., Westrich, J.T., Reaves, C.M., Berner, R.A., 1986. The use of chromium reduction in the analysis of reduced inorganic sulfur in sediments and shales. Chemical Geology 54, 149–155.

Canfield, D.E., Raiswell, R., Bottrell, S., 1992. The reactivity of sedimentary iron minerals toward sulfide. American Journal of Science 292, 659–683.

Canfield, D.E., Habicht, K.S., Thamdrup, B., 2000. The Archean sulfur cycle and the early history of atmospheric oxygen. Science 288, 658–661.

Chambers, L.A., Trudinger, P.A., 1978. Microbiological fractionation of stable sulfur isotopes: a review and critique. Geomicrobiology Journal 1, 249–293.

Chanton, J.P., 1985. Sulfur mass balance and isotopic fractionation in an anoxic marine sediment. Dissertation, University of North Carolina at Chapel Hill.

Chanton, J.P., Martens, C.S., Goldhaber, M.B., 1987. Biogeochemical cycling in an organic-rich coastal marine basin. 8. A sulfur isotopic budget balanced by differential diffusion across the sediment–water interface. Geochimica et Cosmochimica Acta 51, 1201–1208.

Chanton, J.P., Martens, C.S., Paull, C.K., Coston, J.A., 1993. Sulfur isotope and porewater geochemistry of Florida escarpment seep sediments. Geochimica et Cosmochimica Acta 57, 1253–1266.

Claypool, G.E., Holder, W.T., Kaplan, I.R., Sakai, H., Zak, I., 1980. The age curves of sulfur and oxygen isotopes in marine sulfate and their mutual interpretations. Chemical Geology 28, 199–260.

Cline, J.D., 1969. Spectrophotometric determination of hydrogen sulfide in natural waters. Limnology and Oceanography 14, 454–458.

Commeau, R.F., Paull, C.K., Commeau, J.A., Poppe, L.J., 1987. Chemistry and mineralogy of pyrite-enriched sediments at a passive margin sulfide brine seep: abyssal Gulf of Mexico. Earth and Planetary Science Letters 82, 62–74.

Craig, H., 1953. The geochemistry of stable carbon isotopes. Geochimica et Cosmochimica Acta 3, 53–92.

Dale, A.W., Bruchert, V., Alperin, M., Regnier, P., 2009. An integrated sulfur isotope model for Namibian shelf sediments. Geochimica et Cosmochimica Acta 73, 1924–1944.

Deines, P., 1980. The isotopic composition of reduced organic carbon. In: Fritz, P., Fontes, J.C. (Eds.), Handbook of Environmental Isotope Geochemistry. The Terrestrial Environment, vol. 1. A. Elsevier, New York, pp. 329–406.

Dickens, G.R., 2001. Sulfate profiles and barium fronts in sediment on the Blake Ridge. Present and past methane fluxes through a large gas hydrate reservoir. Geochimica et Cosmochimica Acta 65, 529–543.

Dickens, G.R., Snyder, G.T., 2009. Interpreting upward methane flux from marine pore water profiles. Fire in the Ice 9 (1), 7–10.

Doi, H., Kikuchi, E., Mizota, C., Satoh, N., Shikano, S., Yurlova, N., Yadrenkina, E., Zuykova, E., 2004. Carbon, nitrogen, and sulfur isotope changes and hydrogeological processes in a saline lake chain. Hydrobiologia 529, 225–235.

Elsgaard, L., Jorgensen, B.B., 1992. Anoxic transformations of radiolabeled hydrogen sulfide in marine and freshwater sediments. Geochimica et Cosmochimica Acta 56, 2425–2435.

Fossing, H., Jorgensen, B.B., 1990. Oxidation and reduction of radiolabeled inorganic sulfur compounds in an estuarine sediment. Geochimica et Cosmochimica Acta 54, 2731–2742.

Gieskes, J.M., Gamo, T., Brumsack, H., 1991. Chemical methods for interstitial water analysis aboard JOIDES resolution. Ocean Drilling Program Technical Note No. 15.

Goldhaber, M.B., Kaplan, I.R., 1974. The sulfur cycle. In: Goldberg, E.D. (Ed.), The Sea, Marine Chemistry, vol. 5. John Wiley and Sons, New York, pp. 569–655.

Goldhaber, M.B., Kaplan, I.R., 1980. Mechanisms of sulfur incorporation and isotope fractionation during early diagenesis in sediments of the Gulf of California. Marine Chemistry 9, 95–143.

Habicht, K.S., Canfield, D.E., 2001. Isotope fractionation by sulfate-reducing natural populations and the isotopic composition of sulfide in marine sediments. Geology 29, 555–558.

Hinrichs, K.-U., Boetius, A., 2003. The anaerobic oxidation of methane: new insights in microbial ecology and biochemistry. In: Wefer, G., Billett, D., Hebbeln, D., Jorgensen, B.B., Schluter, M., van Weering, T. (Eds.), Ocean Margin Systems. Springer, Berlin, pp. 457–477.

Hoehler, T.M., Alperin, M.J., Albert, D.B., Martens, C.S., 1994. Field and laboratory studies of methane oxidation in anoxic marine sediment: evidence for a methanogen-sulfate reducer consortium. Global Biogeochemical Cycles 8, 451–463.

Hoehler, T.M., Borowski, W.S., Alperin, M.J., Rodriguez, N.M., Paull, C.K., 2000. Model, stable isotope, and radiotracer characterization of anaerobic methane oxidation in the gas-hydrate bearing sediments of the Blake Ridge. In: Paull, Matsumoto, R., Wallace, P.J., Dillon, W.P. (Eds.), Gas Hydrate Sampling on the Blake Ridge and Carolina Rise. Proceedings ODP, Scientific Results, vol. 164, pp. 79–85. College Station, TX.

Holt, B.D., Engelkemeir, A.G., 1970. Thermal decomposition of barium sulfate to sulfur dioxide for mass spectrometric analysis. Analytical Chemistry 42, 1451–1453.

Jorgensen, B.B., 1979. A theoretical model of the stable sulfur isotopic distribution in marine sediments. Geochimica et Cosmochimica Acta 43, 363–374.

Jorgensen, B.B., 1983. The microbial sulfur cycle. In: Krumbein, W.E. (Ed.), Microbial Geochemistry. Blackwell Scientific Publications, St. Louis, pp. 91–124.

Jorgensen, B.B., Bottcher, M.E., Luschen, H., Neretin, L.N., Volkov, I.I., 2004. Anaerobic methane oxidation and a deep H_2S sink generate isotopically heavy sulfides in Black Sea sediments. Geochimica et Cosmochimica Acta 68, 2095–2118.

Kaplan, I.R., Emery, K.O., Rittenberg, S.C., 1963. The distribution and isotopic abundance of sulphur in recent marine sediments off southern California. Geochimica et Cosmochimica Acta 27, 297–331.

Kasten, S., Freudenthal, T., Gingele, F.X., Schulz, H.D., 1998. Simultaneous formation of iron-rich layers at different redox boundaries in sediments of the Amazon deep-sea fan. Geochimica et Cosmochimica Acta 62, 2253–2264.

Kastner, M., Torres, M., Solomon, E., Spivack, 2008. Marine pore fluid profiles of dissolved sulfate: do they reflect *in situ* methane fluxes? Fire in the Ice 8 (3), 6–8.

Manheim, F.T., 1966. A Hydraulic Squeezer for Obtaining Interstitial Water from Consolidated and Unconsolidated Sediments. U.S. Geological Survey Professional Paper 550-C, pp. 256–261.

Middleburg, J.J., 1991. Organic carbon, sulphur, and iron in recent semi-euxinic sediments of Kau Bay, Indonesia. Geochimica et Cosmochimica Acta 55, 815–828.

Morse, J.W., Cornwell, J.C., 1987. Analysis and distribution of iron sulfide minerals in recent anoxic marine sediments. Marine Chemistry 22, 55–69.
Naehr, T.N., Rodriguez, N.M., Bohrmann, G., Paull, C.K., Botz, R., 2000. Methane-derived authigenic carbonates associated with gas hydrate decomposition and fluid venting above the Blake Ridge Diapir. In: Paull, Matsumoto, R., Wallace, P.J., Dillon, W.P. (Eds.), Gas Hydrate Sampling on the Blake Ridge and Carolina Rise. Proceedings ODP, Scientific Results, vol. 164, pp. 285–300. College Station, TX.
Nakai, N., Jensen, M.L., 1964. The kinetic isotope effect in the bacterial reduction and oxidation of sulfur. Geochimica et Cosmochimica Acta 28, 1893–1912.
Niewohner, C., Henson, C., Kasten, S., Zabel, M., Schultz, H.D., 1998. Deep sulfate reduction completely mediated by anaerobic methane oxidation in sediments of the upwelling area off Nambia. Geochimica et Cosmochimica Acta 62, 455–464.
Nriagu, J.O., Coker, R.D., 1983. Sulphur in sediments chronicles past changes in lake acidification. Nature 303, 692–694.
Okada, H., 2000. Neogene and Quaternary calcareous nannofossils from the Blake Ridge, Sites 994, 995, and 997. In: Paull, Matsumoto, R., Wallace, P.J., Dillon, W.P. (Eds.), Gas Hydrate Sampling on the Blake Ridge and Carolina Rise. Proceedings ODP, Scientific Results, vol. 164, pp. 331–341. College Station, TX.
Orphan, V.J., House, C.H., Hinrichs, K., McKeegan, K.D., DeLong, E.F., 2001. Methane-consuming Archaea revealed by directly coupled isotopic and phylogenetic analysis. Science 293, 484–487.
Pancost, R.D., Hopmans, E.C., Sinninghe Damste, J.S., Medinaut Shipboard Scientific Party, 2001. Archaeal lipids in Mediterranean cold seeps: molecular proxies for anaerobic methane oxidation. Geochimica et Cosmochimica Acta 65, 1611–1627.
Passier, H.F., Middleburg, J.J., van Os, B.J.H., de Lange, G.J., 1996. Diagenetic pyritisation under eastern Mediterranean sapropels caused by downward sulfide diffusion. Geochimica et Cosmochimica Acta 60 (5), 751–763.
Paull, C.K., Neumann, A.C., 1987. Continental margin brine seeps: their geological consequences. Geology 15, 545–548.
Paull, C.K., Matsumoto, R., Wallace, P.J., et al., 1996. Proceedings ODP, Initial Reports, vol. 164, College Station, Texas, Ocean Drilling Program.
Paull, C.K., Lorenson, T.D., Borowski, W.S., Ussler III, W., Olsen, K., Rodriguez, N.M., 2000. Isotopic composition of CH_4, CO_2 species, and sedimentary organic matter within samples from the Blake Ridge: Gas source implications. In: Paull, Matsumoto, R., Wallace, P.J., Dillon, W.P. (Eds.), Gas Hydrate Sampling on the Blake Ridge and Carolina Rise. Proceedings ODP, Scientific Results, vol. 164, pp. 67–78. College Station, TX.
Paytan, A., Kastner, M., Campbell, D., Thiemens, M.H., 1998. Sulfur isotopic composition of Cenozoic seawater sulfate. Science 282, 1459–1462.
Price, F.T., Shieh, Y.N., 1979. Fractionation of sulfur isotopes during laboratory synthesis of pyrite at low temperatures. Chemical Geology 27, 245–253.
Raiswell, R., 1988. Chemical model for the origin of minor limestone-shale cycles by anaerobic methane oxidation. Geology 16, 641–644.
Reeburgh, W.S., 1967. An improved interstitial water sampler. Limnology and Oceanography 12, 163–165.
Reeburgh, W.S., 1976. Methane consumption in Cariaco Trench waters and sediments. Earth and Planetary Science Letters 28, 337–344.
Reeburgh, W.S., 1983. Rates of biogeochemical processes in anoxic sediments. Annual Review of Earth and Planetary Sciences 11, 269–298.
Rees, C.E., Jenkins, W.J., Monster, J., 1978. The sulphur isotopic composition of ocean water sulphate. Geochimica et Cosmochimica Acta 42, 377–381.
Rickard, D., 1997. Kinetics of pyrite formation by the H_2S oxidation of iron (II) monosulfide in aqueous solutions between 25 and 125°C: the rate equation. Geochimica et Cosmochimica Acta 61, 115–134.
Rickard, D., Luther III, G.W., 1997. Kinetics of pyrite formation by the H_2S oxidation of iron (II) monosulfide in aqueous solutions between 25 and 125°C: the mechanism. Geochimica et Cosmochimica Acta 61, 135–147.
Rodriguez, N.M., Paull, C.K., Borowski, W.S., 2000. Zonation of authigenic carbonates within gas-hydrate-bearing sedimentary sections on the Blake Ridge, offshore southeastern North America. In: Paull, Matsumoto, R., Wallace, P.J., Dillon, W.P. (Eds.), Gas Hydrate Sampling on the Blake Ridge and Carolina Rise. Proceedings ODP, Scientific Results, vol. 164, pp. 301–312. College Station, TX.
Rudnicki, M.D., Elderfield, H., Spiro, B., 2001. Fractionation of sulfur isotopes during bacterial sulfate reduction in deep ocean sediments at elevated temperatures. Geochimica et Cosmochimica Acta 65, 777–789.
Schultz, H.D., Dahmke, A., Schinzel, U., Wallmann, K., Zabel, M., 1994. Early diagenetic processes, fluxes, and reaction rates in sediments of the South Atlantic. Geochimica et Cosmochimica Acta 58, 2041–2060.
Sim, M.S., Bosak, T., Ono, S., 2011. Large sulfur isotope fractionation does not require disproportion. Science 333, 74–77.
Snyder, G.T., Dickens, G.R., Tomaru, H., Takeuchi, R., Komatsubara, J., Ishida, Y., Yu, H., 2007a. Pore water profiles and authigenic mineralization in shallow marine sediments above the methane-charged system on Umitaka Spur, Japan Sea. Deep-Sea Research. Part II: Topical Studies in Oceanography 54 (11–13), 1216–1239.
Snyder, G.T., Dickens, G.R., Castellini, D.G., 2007b. Labile barite contents and dissolved barium concentrations on Blake Ridge: new perspectives on barium cycling above gas hydrates. Journal of Geochemical Exploration 95, 48–65.
Sternbeck, J., Sohlenius, G., 1997. Authigenic sulfide and carbonate mineral formation in Holocene sediments of the Black Sea. Chemical Geology 135, 55–73.
Strauss, H., 1999. Geological evolution from isotope proxy signals – sulfur. Chemical Geology 161, 89–101.
Thiel, V., Peckmann, J., Richnow, H.H., Luth, U., Reitner, J., Michaelis, W., 2001. Molecular signals for anaerobic methane oxidation in Black Sea seep carbonates and a microbial mat. Marine Chemistry 73, 97–112.
Torres, M.E., Brumsack, H.J., Bohrmann, G., Emeis, K.C., 1996. Barite fronts in continental margin sediments: a new look at barium remobilization in the zone of sulfate reduction and formation of heavy barites in diagenetic fronts. Chemical Geology 127, 125–139.
Ussler III, W., Paull, C.K., 2008. Rates and consequences of anaerobic oxidation of methane and authigenic carbonate precipitation in deep-sea sediments inferred from porewater chemical profiles. Earth and Planetary Science Letters 226, 271–287.
Valentine, D.L., Reeburgh, W.S., 2000. New perspectives on anaerobic methane oxidation. Environmental Microbiology 2, 477–484.
Wang, J., Chen, Q., Wei, Q., Wang, X., Li, Q., Gao, Y., 2008. Authigenic pyrites and their stable sulfur isotopes in sediments from IODP 311 on Cascadia margin, Northeastern Pacific. In: Proceedings 6th International Conference Gas Hydrates.
Weiss, R.F., Craig, H., 1973. Precise shipboard determination of dissolved nitrogen, oxygen, argon, and total inorganic carbon by gas chromatography. Deep-Sea Research 20, 291–303.
Wilkin, R.T., Barnes, H.L., 1996. Pyrite formation by reactions of iron monosulfides with dissolved inorganic and organic sulfur species. Geochimica et Cosmochimica Acta 60, 4167–4179.
Woese, C.R., Fox, G.E., 1977. Phylogenetic structure of the prokaryotic domain: the primary kingdoms. Proceedings of the National Academy of Sciences of the United States of America 74, 5088–5090.
Wortmann, U.G., the Expedition 311 Scientists, 2008. Data report: $\delta^{34}S$ and $\delta^{18}O$ measurements of dissolved sulfate from interstitial water samples, IODP Expedition 311. In: Riedel, M., Collett, T.S., Malone, M.J. (Eds.), Proceedings of the Integrated Ocean Drilling Program, vol. 311. Integrated Ocean Drilling Program Management International, Inc, Washington, DC. http://dx.doi.org/10.2204/iodp.proc.311.209.2008.
Wortmann, U.G., Bernasconi, S.M., Bottcher, M.E., 2001. Hypersulfidic deep biosphere indicates extreme sulfur isotope fractionation during single-step microbial sulfate reduction. Geology 29, 647–650.
Zhabina, N.N., Volkov, I.I., 1978. A method for the determination of various sulfur compounds in sea sediments and rocks. In: Krumbein, W.E. (Ed.), Environmental Biogeochemistry: Methods, Metals, and Assessment, vol. 3. Ann Arbor Science Publishers, Ann Arbor, pp. 735–746.
Zhang, C.L., Li, Y., Wall, J.D., Larsen, L., Sassen, R., Huang, Y., Peacock, A., White, D.C., Horita, J., Cole, D.R., 2002. Lipid and carbon isotopic evidence of methane-oxidizing and sulfate-reducing bacteria in association with gas hydrates from the Gulf of Mexico. Geology 30, 239–242.